Supporting Information

Engineering Regiospecific Methylation of the Pladienolides

Emily R. Smith,[a,†] Dua H. Al-Smadi,[b, c,†] Yitao Dai,[b] Manead Khin,[b] Joanna Burdette,[b] Brendan M. Duggan,[d] James J. La Clair,[a] Alessandra S. Eustáquio,*[b] and Michael D. Burkart,*[,a]

[a] Department of Chemistry and Biochemistry, University of California, San Diego, 9500 Gilman Drive, La Jolla CA 92093-0358, United States

[b] Department of Pharmaceutical Sciences, College of Pharmacy, University of Illinois at Chicago, Chicago, IL 60607, United States

[c] Department of Medicinal Chemistry and Pharmacognosy, College of Pharmacy, Jordan University of Science and Technology, Irbid, 22110, Jordan

[d] Skaggs School of Pharmacy and Pharmaceutical Sciences, UC San Diego, 9500 Gilman Drive, La Jolla, California, 92093, United States.

[*] Corresponding authors: Michael D. Burkart (UC San Diego) email: mburkart@ucsd.edu and Alessandra S. Eustáquio (UIC) email: ase@uic.edu

Table of Contents

Evaluation of the herboxidiene *O*-methyltransferase.

We first attempted to achieve *O*-methylation via introduction of the *O*-methyltransferase gene *herF* from the herboxidiene (**5**) producer *S. chromofuscus* (Fig. S1)[30] to *S. platensis*. We then applied Atomic Sort[31] to evaluate the products of the engineered strains.

The *herF* gene was amplified by PCR from *S. chromofuscus* genomic DNA and ligated into an integrative (φC31) pSET152-based vector under the control of the constitutive *ermE** promoter to generate pYD001 (Table S1). Because *herF* is translationally coupled with the upstream *herE* gene that encodes an epoxidase (Fig. S1), we also evaluated an alternative design in which *herEF* was cloned under control of the *ermE** promoter to generate pYD005. *S. platensis* mutant strains containing either pYD001 or pYD005 were obtained via conjugation from *E. coli* S17.1 and apramycin selection as previously described.[16] Mutants were confirmed by PCR (Figs. S2–S3).

S. platensis wild-type and mutant strains were cultivated in SPCGB production medium at 25 °C for five days as previously described.[16] EtOAc extracts of whole cultures were prepared. We also evaluated defatting using hexanes (Fig. S4). Extracts were analyzed by HPLC in comparison with an authentic standard of pladienolide B (**2**) (Figs. S5–S6) and no new products were identified.

Using Acceleration by Sharing of Adjacent Polarization (ASAP),[32] we collected multiplicity-edited ^{1}H,^{13}C-HSQC spectra on 200±50 µg samples of each extract dissolved in 35 µL of d_6 benzene. Spectra were referenced to the residual protonated benzene peak and peak picked. The ^{1}H and ^{13}C chemical shifts and intensity of each peak were used as input for the Atomic Sort algorithm.[31] Previously, the Atomic Sort was used to find the most distant peaks.[31] Here, the algorithm was used to find the closest peaks as described previously.[33] Briefly, by comparing the spectrum of a culture against a collection of reference spectra a score was calculated for how closely each reference spectrum matched the query culture spectrum. Sorting these scores identified the spectra, and thus the compounds, most likely to be present in the query culture. The great strength of this approach is that it maps reference atoms to query atoms. In cases where related metabolites are present, the algorithm will identify the shared structural fragments and highlight the location of modifications.

Evaluation of the success of different biosynthetic constructs not only requires identifying the products but determining their concentration. To this end we used the Atomic Sort[32] to identify the most distant peaks of each metabolite by comparing its peaks against the peaks of all the other metabolites. Once the most distinctive peaks were identified, integration and comparison with the integral of the residual protonated solvent enabled estimation of the concentration of the metabolites. While the interpretation of HSQC integrals is complicated by variation in *J*-coupling and relaxation, integrals of the same atoms can be compared between spectra collected in the same way.[34] Using this approach, we were able to quantitatively evaluate different cultures. Although no 21-methoxypladienolide B (**8**) product was detected, as summarized in Table S2, both pladienolide B (**2**) and an alkene precursor (lacking epoxidation) were detected in the wild-type strain in approximately 1:1 ratio. Three of four analyzed *herF* containing strains also displayed a ~1:1 ratio of **2** and the alkene precursor (the exception being *herF* clone #5 for which the precursor was not detected). In contrast, for all four analyzed *herEF* containing strains only pladienolide B (**2**) could be detected but not the precursor. These combined results indicate that while HerF is not functional in methylating **2**, the epoxidase HerE may contribute to converting the alkene precursor into **2**, although further studies are required to test this hypothesis.

30 L. Shao, J. Zi, J. Zeng, J. Zhan, J. *Appl. Environ. Microbiol* **2012**, *78*, 2034–2038

31 B. M. Duggan, R. Cullum, W. Fenical, L. A. Amador, A. D. Rodríguez, J. J. La Clair, *Angew. Chem. Int. Ed. Engl*. **2020**, *59*, 1144–1148.

32 D. Schulze-Sünninghausen, J. Becker, B. Luy B. *J. Am. Chem. Soc*. **2014**, *136*, 1242–1245.

33 R. J. Stankey, D. Johnson, B. M. Duggan, D. A. Mead, J. J. La Clair, *Mar. Drugs.* **2023**, *21*, 56.

34 F. Fardus-Reid, J. Warren, A. L. Gresley, *Anal. Methods* **2016**, *8*, 2013–2019.

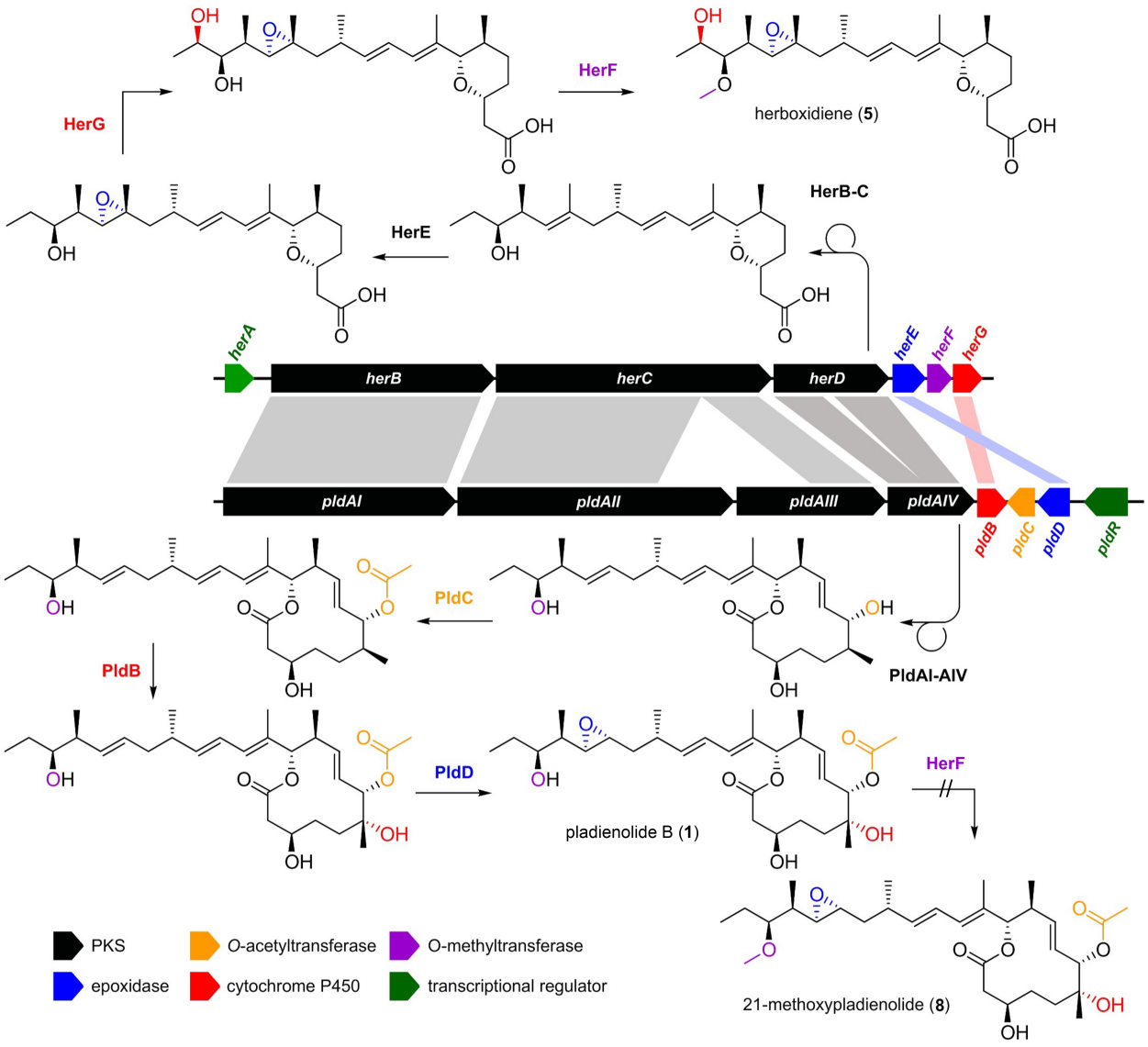

Fig. S1. The pladienolide (*pld*) and herboxidiene (*her*) biosynthetic gene clusters from *S. platensis* Mer-11107 and *S. chromofuscus* ATCC 49982, respectively. Genes are color-coded based on function as indicated. Genes that share sequence similarity between the two clusters are connected through shaded bars. Transfer of either *herF* or *herEF* into the *S. platensis* pladienolide producer was tested in this study to engineer 21-methoxypladienolide B (**8**).

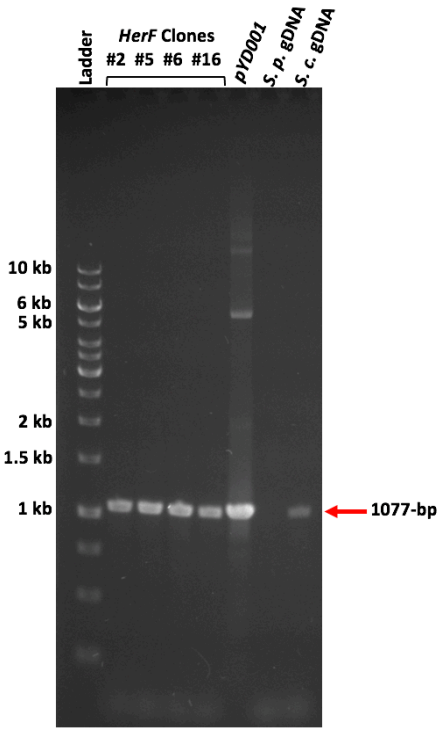

Fig. S2. *PCR results of four individual herF exconjugants*. # indicates the exconjugant number. The expected band of the *herF* amplicon is 1077 bp. *S. chromofuscus* ATCC 49982 (S. c.) genomic DNA (gDNA, source of *herF*) and pYD001 were used as positive controls. *S. platensis* (S. p., parent strain) gDNA was used as the negative control. Ladder, GeneRuler 1kb DNA Ladder from ThermoScientific.

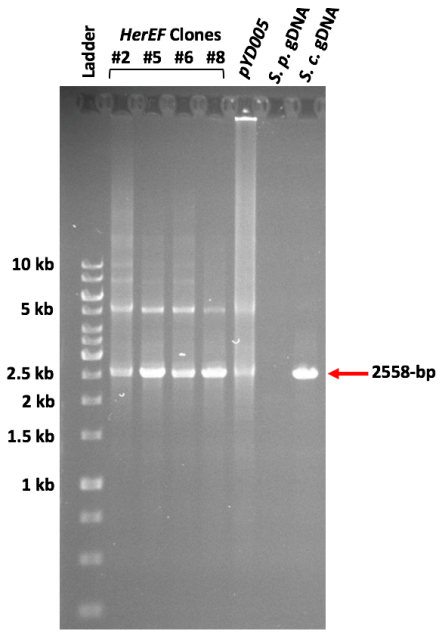

Fig. S3. *PCR results of four individual herEF exconjugants*. # indicates the exconjugant number. The expected band of *herEF* amplicon is 2558 bp. *S. chromofuscus* ATCC 49982 (*S. c.*) gDNA (source of *herEF*) and pYD005 were used as positive controls. *S. platensis* (*S. p.*, parent strain) gDNA was used as the negative control. Additional bands at ~5 kb are potentially caused by unspecific primer binding on the plasmid. Ladder, GeneRuler 1kb DNA Ladder from ThermoScientific.

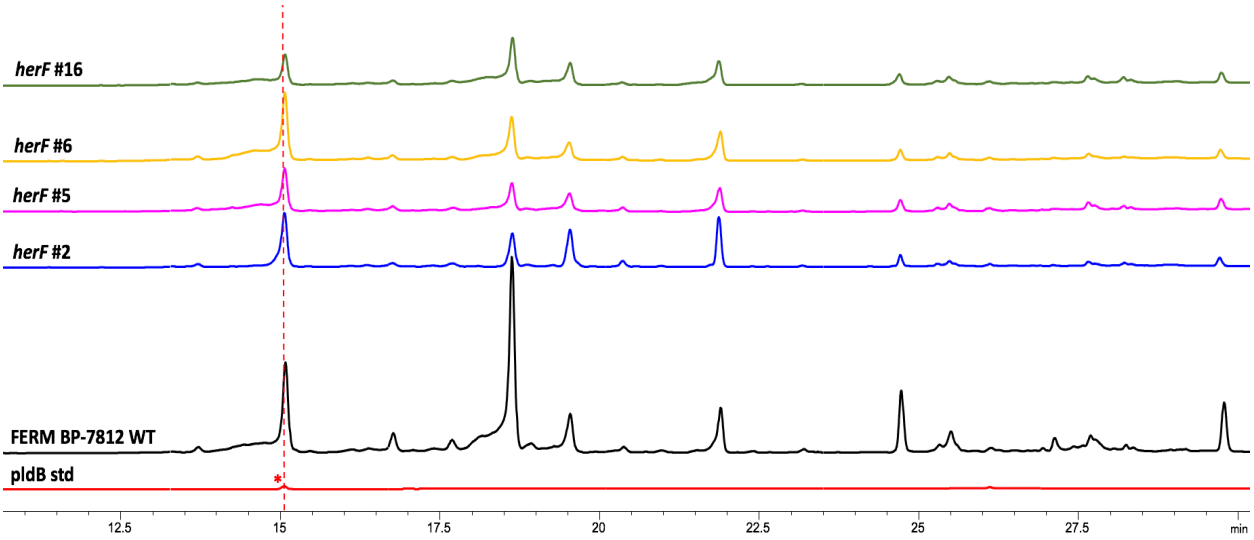

Fig. S4. HPLC chromatograms of four independent *herF* clone extracts, compared to the wild-type (WT) extract, and pladienolide B (**2**) standard (pldB std, 10 µl of a 10 ng/µL solution). The pladienolide B (**2**) peak is highlighted with a red asterisk at 15.1 min. Detection at 240 nm.

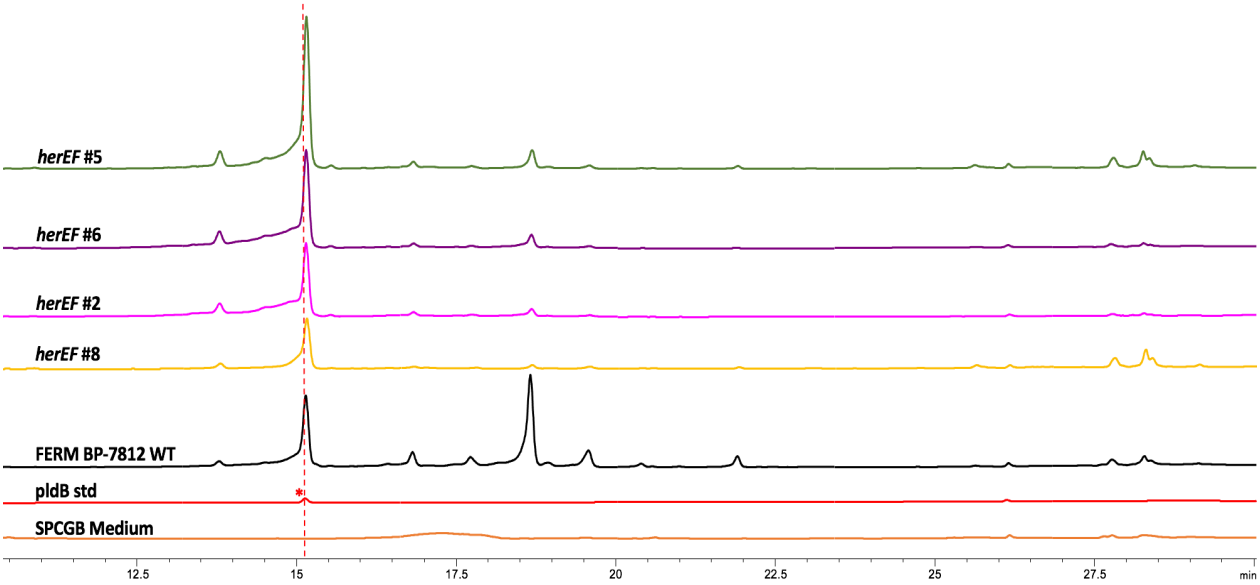

Fig. S5. HPLC chromatograms of four independent *herEF* clone extracts compared to the wild-type (WT) extract, and pladienolide B (**2**) standard (pldB std, 10 µl of a 10 ng/µL solution). The pladienolide B (**2**) peak is highlighted with a red asterisk at 15.1 min. Detection at 240 nm.

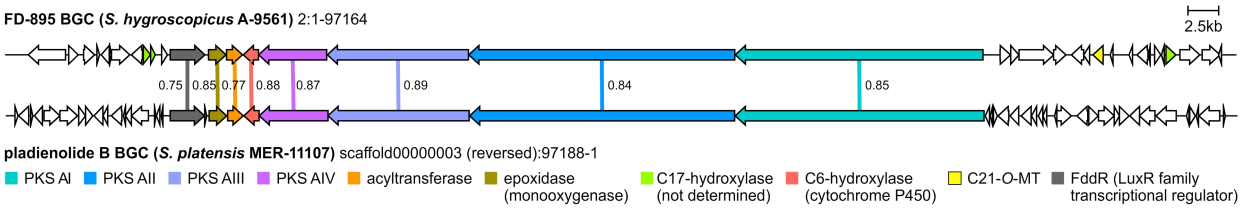

Fig. S6. *FD-895 and pladienolide biosynthetic gene cluster alignment determined with Clinker.* Percent (%) identity of gene pairs is shown between the two corresponding gene clusters (% identity minimum: 30%). Color-coded legend of homologous genes is included at the bottom of the figure.

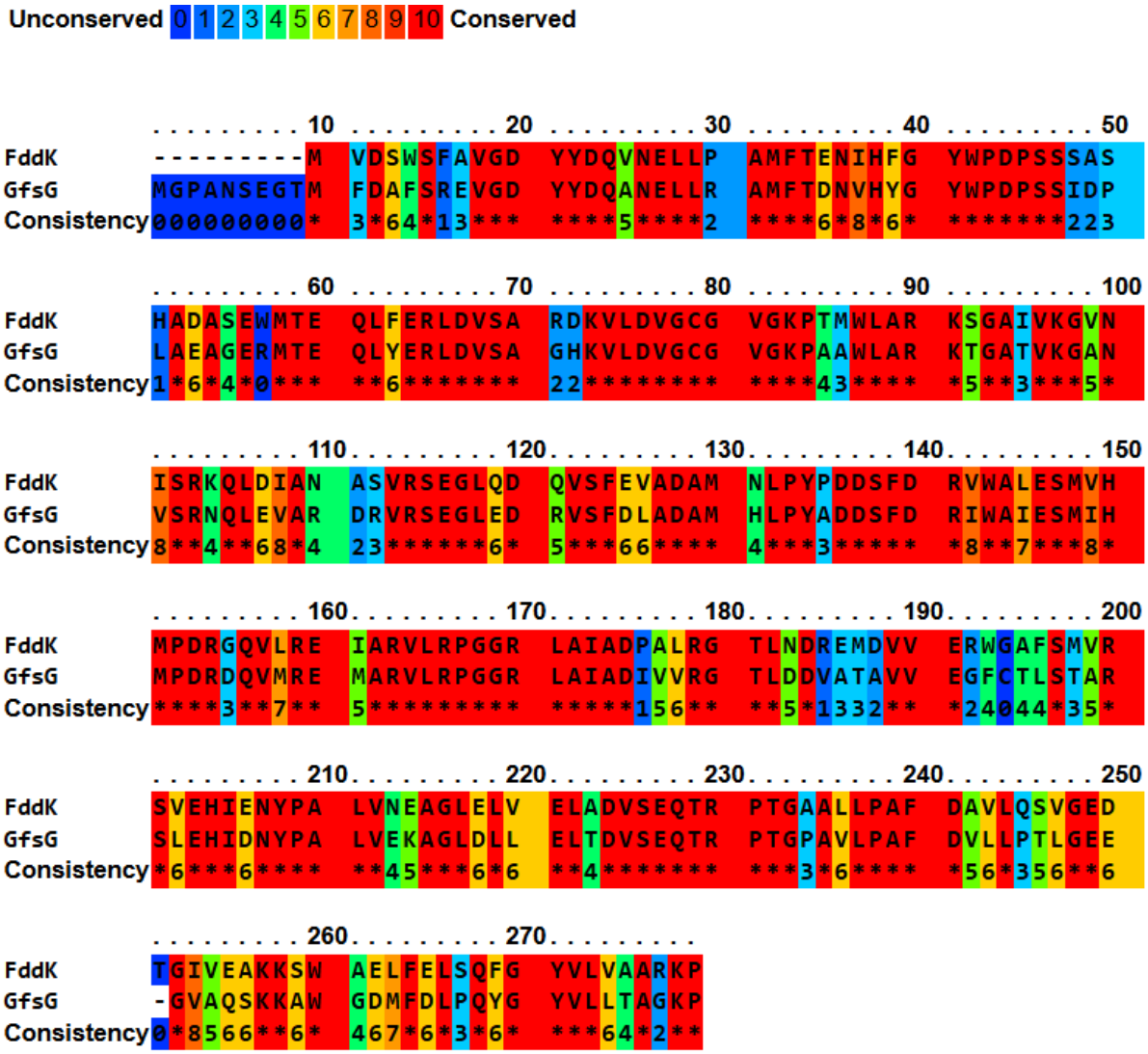

Fig. S7. *FddK and GfsG amino acid sequence alignment*. FddK and GfsG share 67% amino acid sequence identity with a total of 181 identical residues. The coloring follows rainbow order with fully conserved residues in red and the least conserved residues in dark navy blue (see legend). No tags or adapters are included in the sequence alignment.

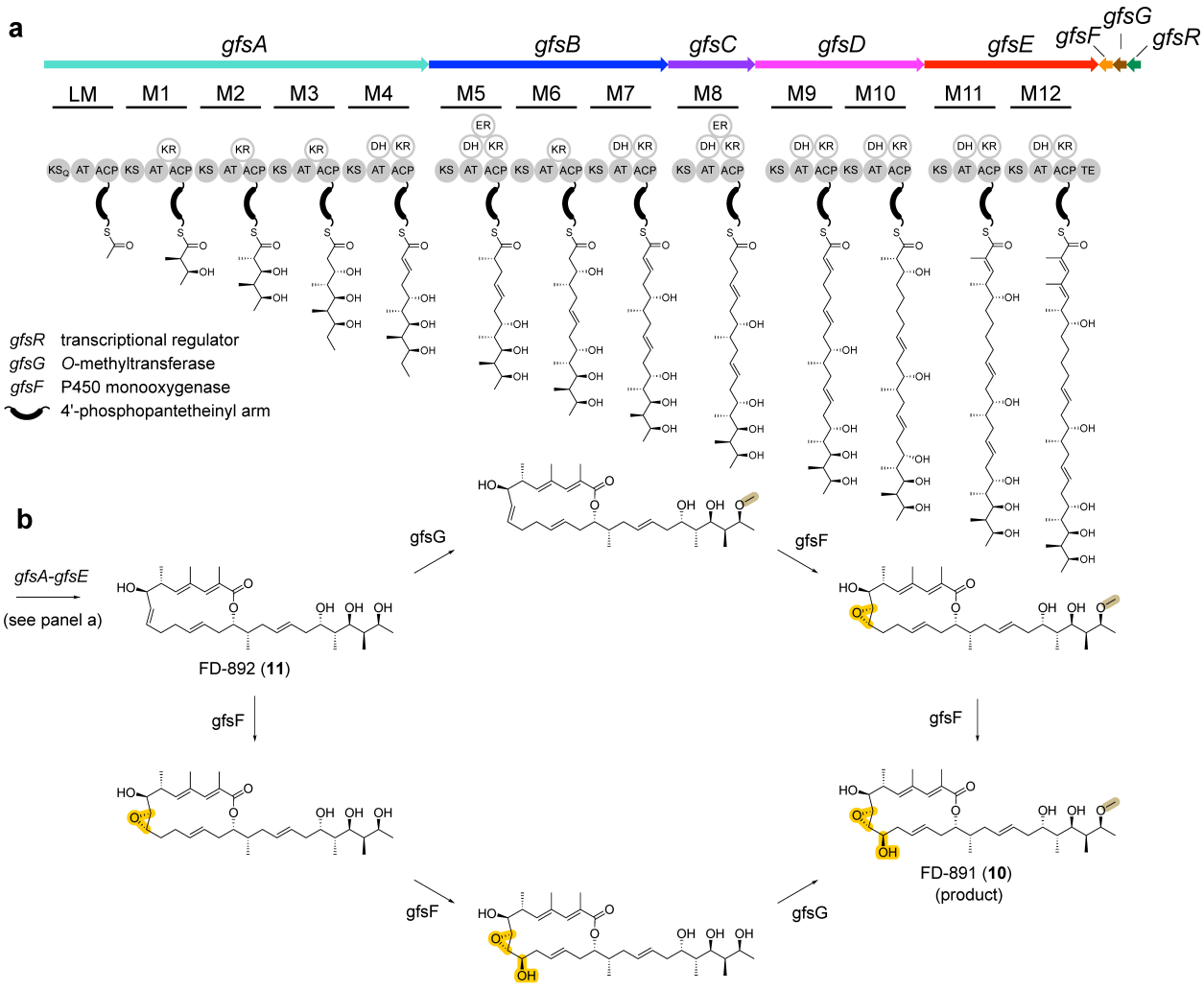

Fig. S8. *FD-891 biosynthesis*. **a)** FD-891 (**10**) BGC from *Streptomyces graminofaciens* A-8890 showing the 13 modules (LM-M12), domain architecture, and tailoring enzymes (GfsF, GfsG, and GfsR). Domains are given by the following abbreviations: ACP, acyl carrier protein; AT, acyltransferase; DH, dehydratase; ER, enoylreductase; KR, ketoreductase; KS, ketosynthase; and TE, thioesterase. **b)** Parallel post-PKS modification pathways include the conversion of FD-892 (**11**, gfsA-gfsE product) to the final product, **10**, however GfsF always catalyzes epoxidation then hydroxylation in a stepwise manner regardless of acting before or after GfsG.[17]

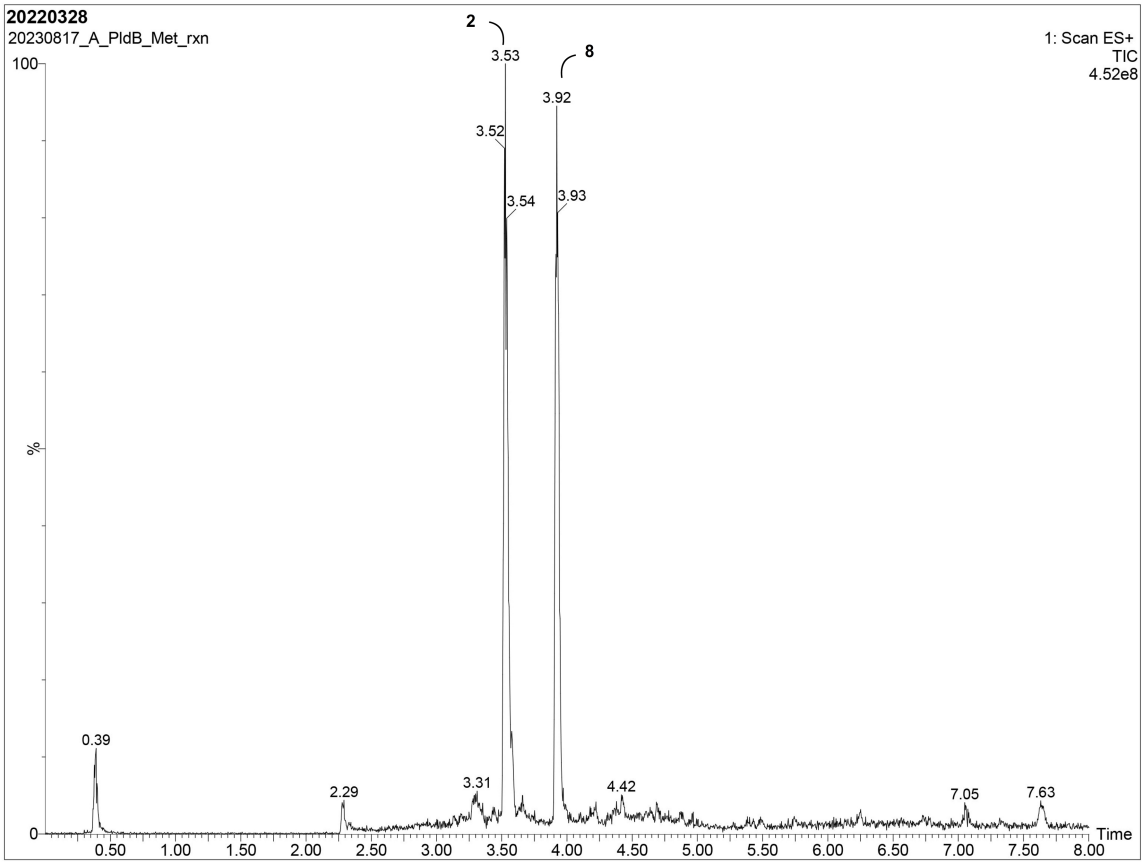

Fig. S9. *LC-MS spectra of crude in vitro production of 21-methoxypladienolide B (**8**).* LC-MS trace of the crude reaction containing two peaks for **2** and **8**.

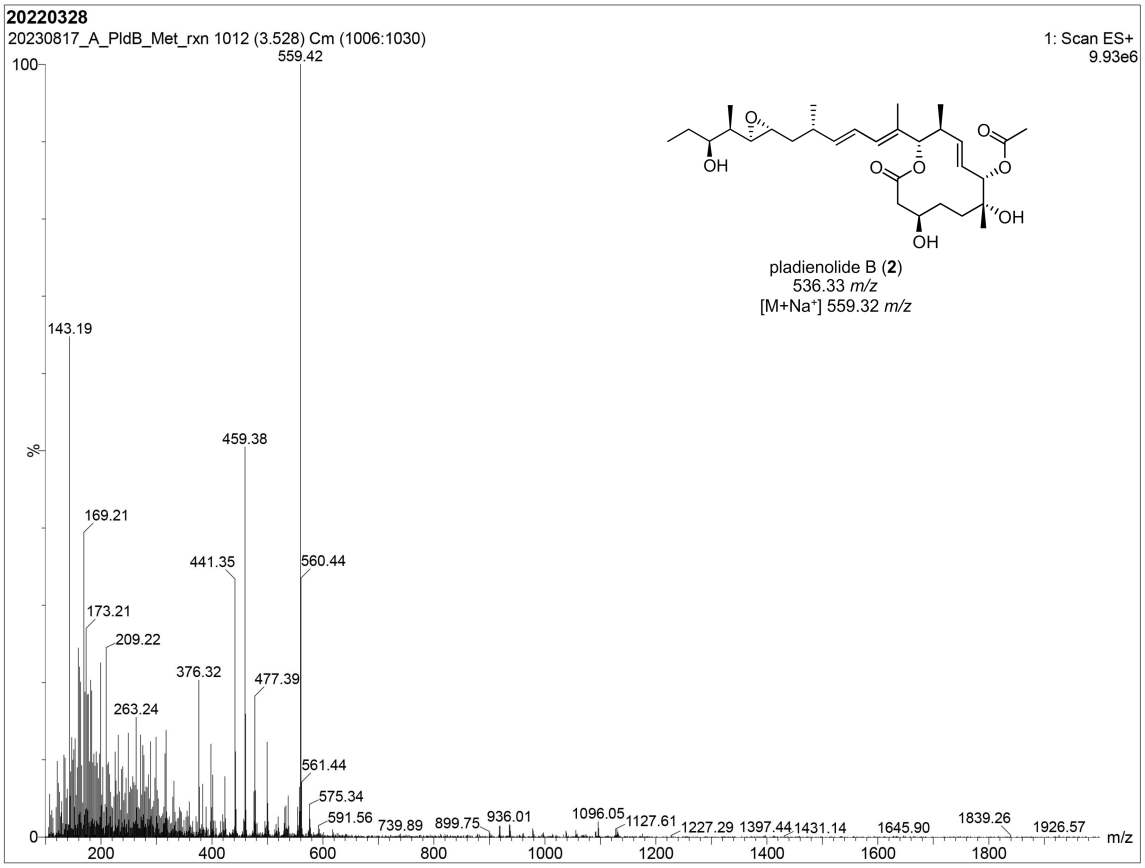

Fig. S10. *LC-MS spectra of crude in vitro production of 21-methoxypladienolide B (**8**)***.** MS data from the LC trace in Fig. S9 showing the mass of **2**.

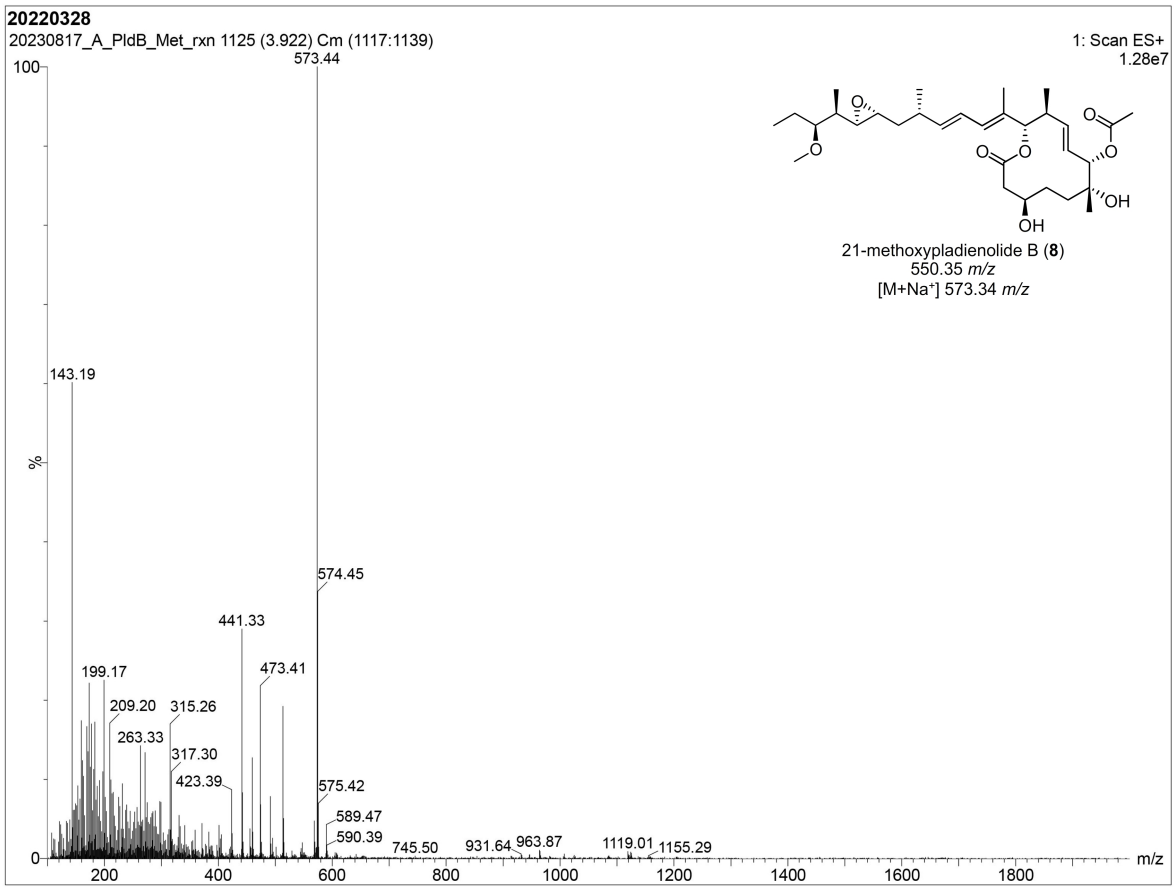

Fig. S11. *LC-MS spectra of crude in vitro production of 21-methoxypladienolide B (**8**)***.** MS data from the LC trace in Fig. S9 showing the mass of **8**.

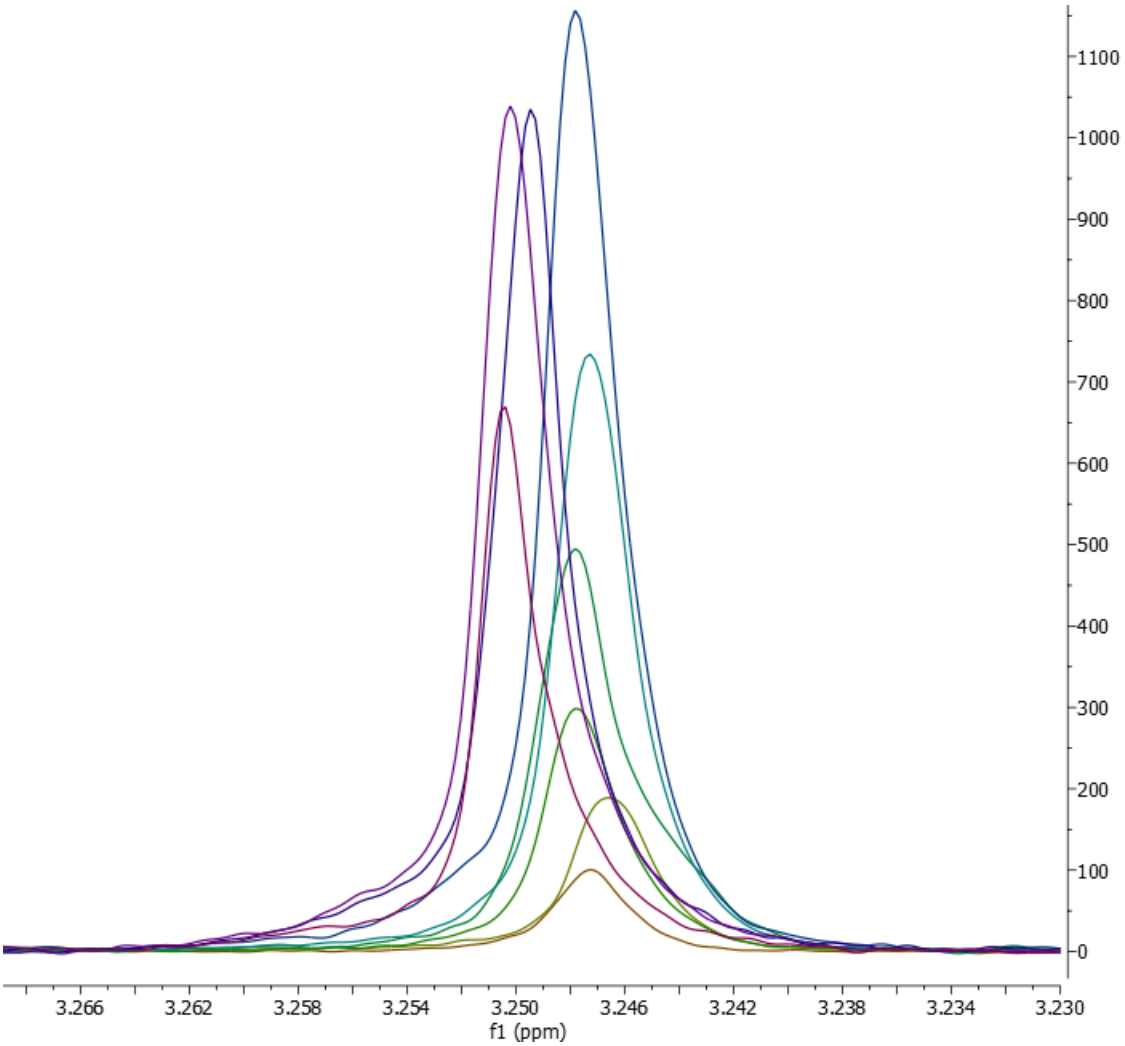

Fig. S12. *In vitro temperature study*. **a)** Overlay of ^{1}H NMR spectra depicting the C21 methoxy group in crude reactions screened at 5 °C intervals from 20 °C to 50 °C, including 37 °C and 42 °C. The peak in navy blue (40 °C) gave the highest relative integration (0.76, Table S3).

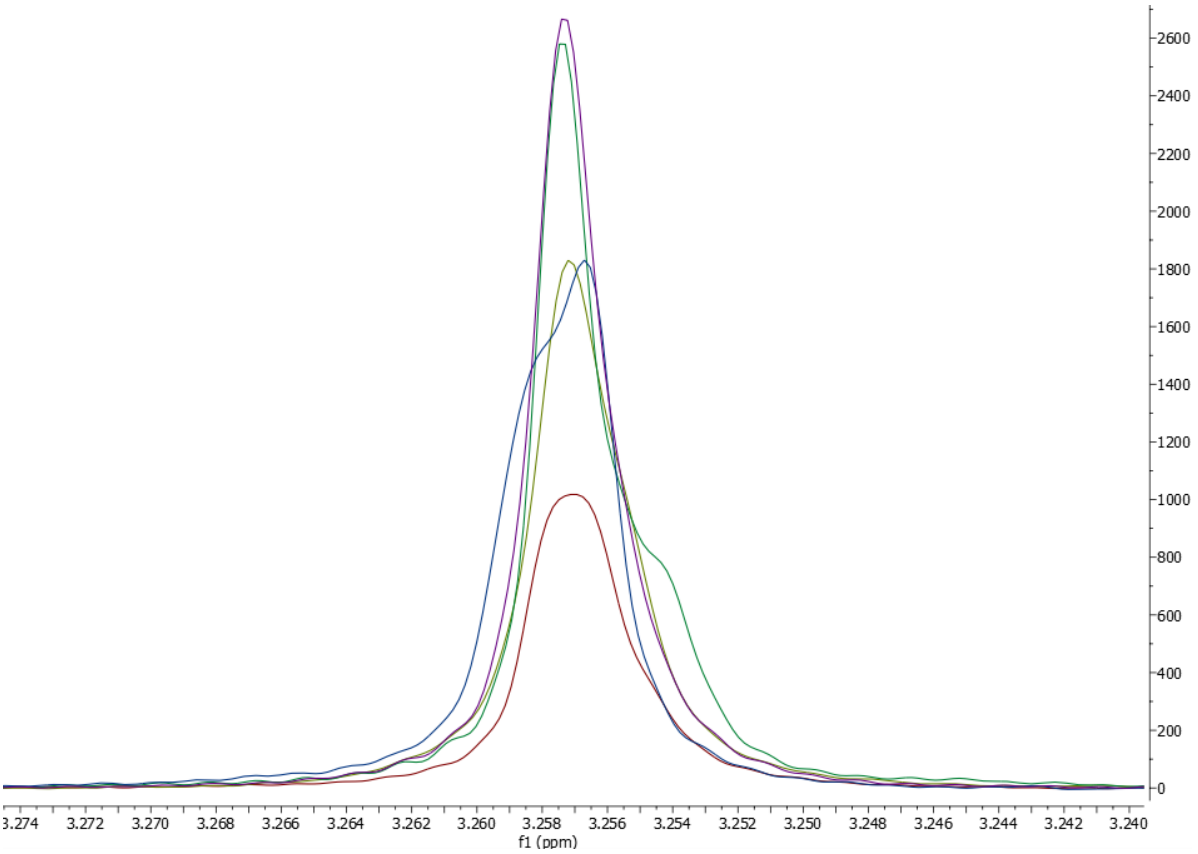

Fig. S13. *In vitro pH study.* Overlay of ^{1}H NMR spectra depicting the C21 methoxy group in crude reactions screened at pH 7.0, 7.3, 7.5, 7.7, and 8.0. The peak in forest green (pH 7.5) gave the highest relative integration (0.89, Table S4).

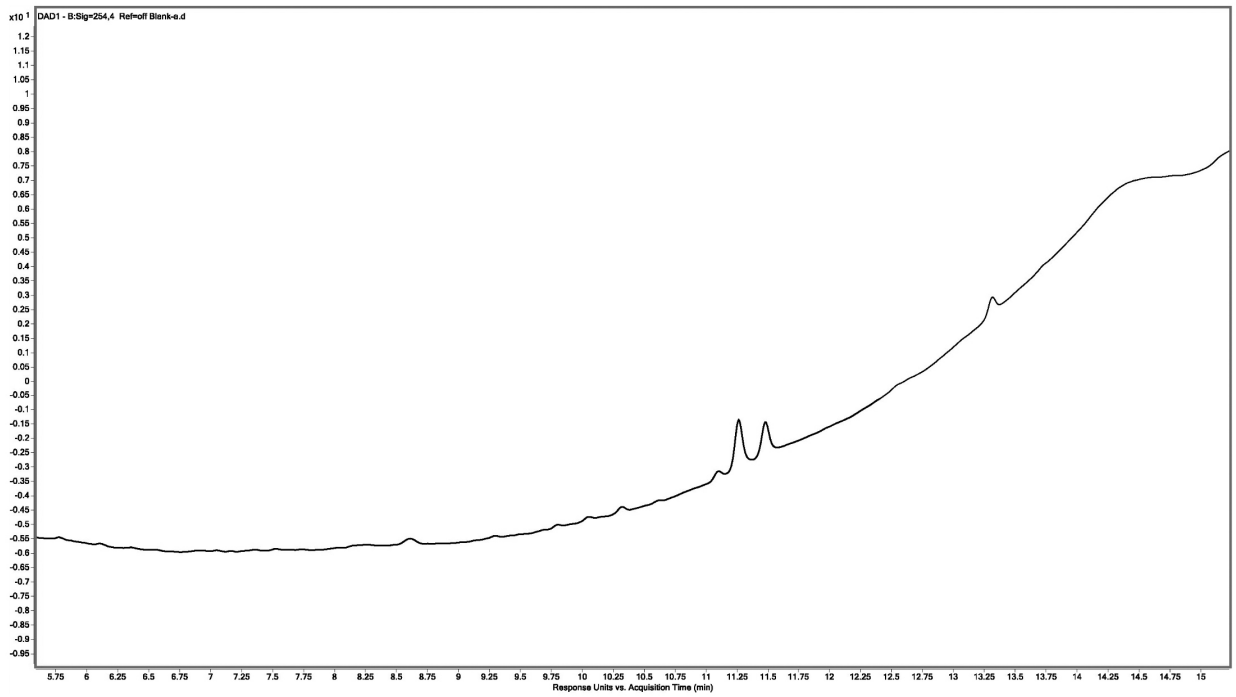

Fig. S14. *Comparison of the in vivo and in vitro production of **8***. LC traces depicting the level of UV absorption at 254 nm from injection of blank. This serves as a control for the data presented in Figs. S15–S17.

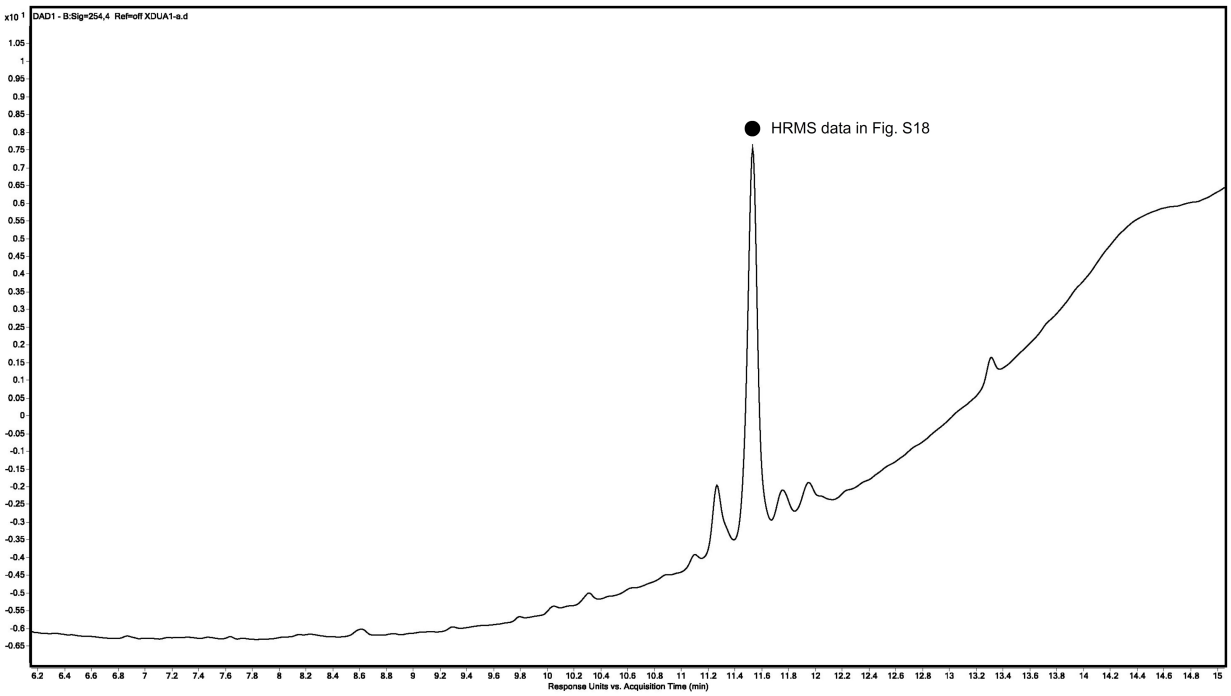

Fig. S15. *The in vivo production of **8***. LC analysis of a sample of **8** produced by the *in vivo* enzymatic approach. This data can be compared to that shown in Figs. S16–S17. Control data is provided in Fig. S14.

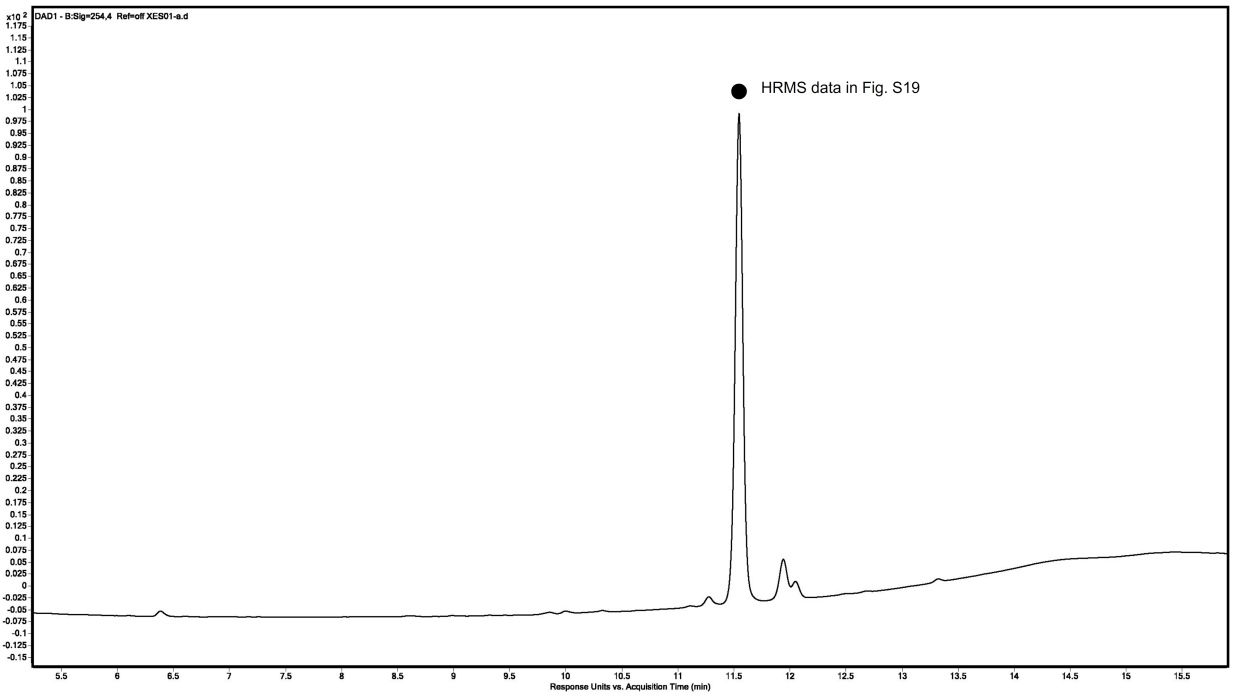

Fig. S16. *The in vitro production of **8**.* LC analyses conducted on a sample of **8** produced by the *in vitro* engineered approach. This data can be compared to that shown in Fig. S15 and Fig. S17. Control data is provided in Fig. S14.

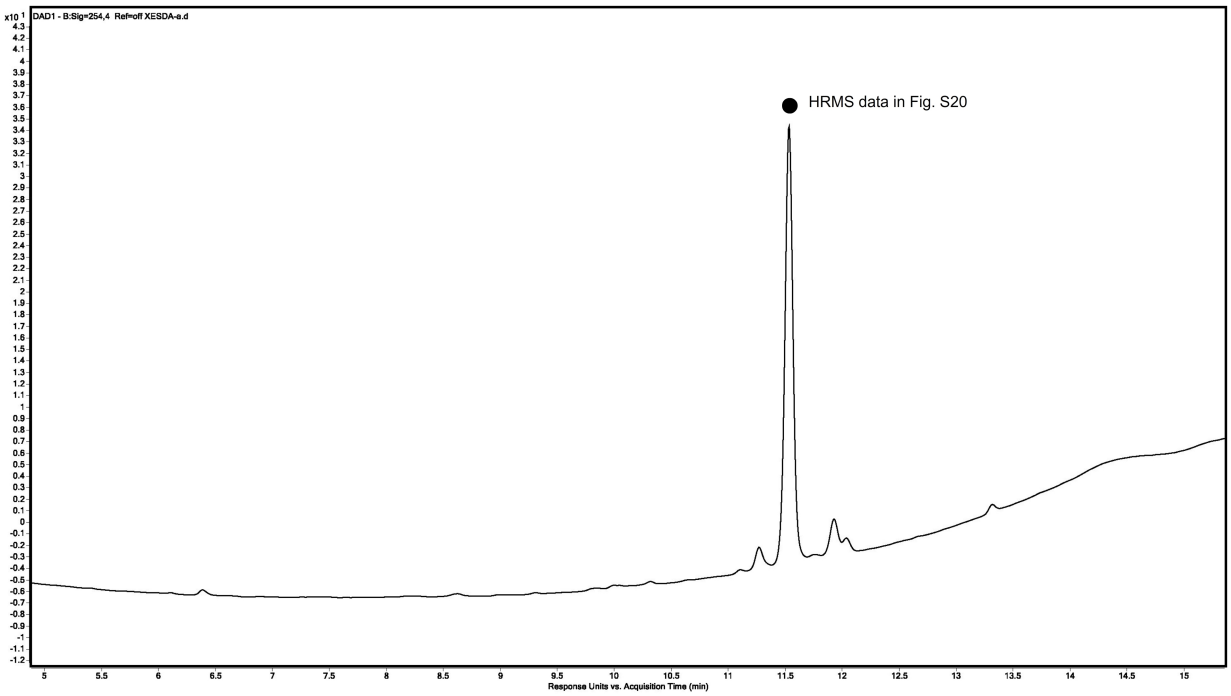

Fig. S17. *Comparison of the in vivo and in vitro production of **8***. LC analyses conducted on a mixture (1:1 v:v) of **8** produced by the *in vitro* enzymatic approach and **8** produced by the *in vivo* engineered approach. This data can be compared to that shown in Figs. S15–S16. Control data is provided in Fig. S14.

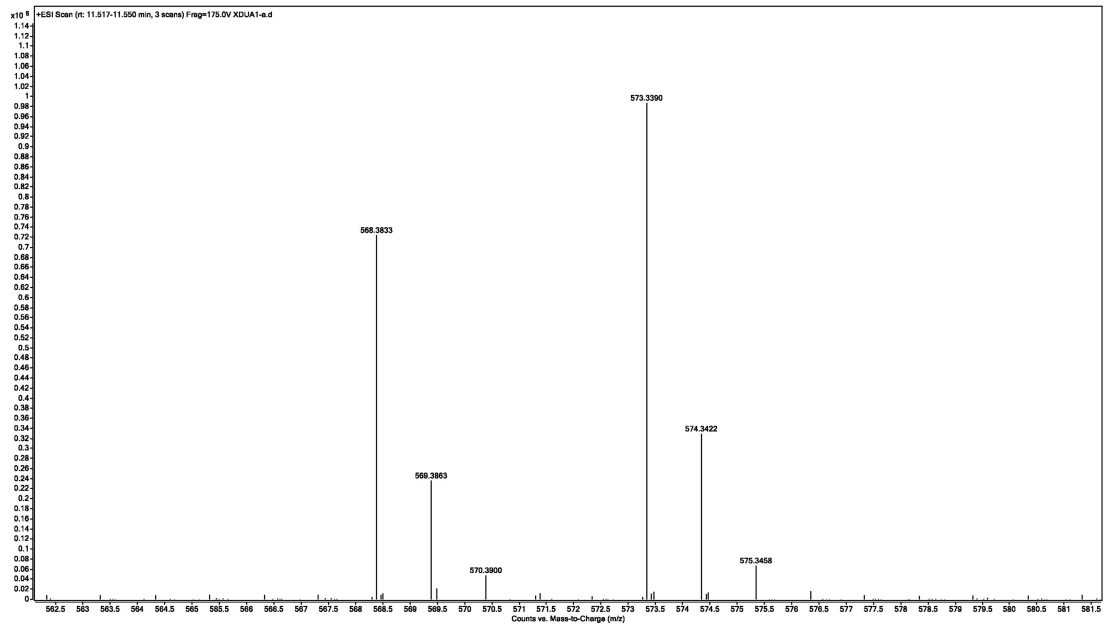

Search Results:

Mass Measured	Theo. Mass	Delta (ppm)	Composition
568.3833	568.3844	-1.9	$[C_{31}H_{50}O_8NH_4]^+$
573.3390	573.3398	-1.4	$[C_{31}H_{50}O_8Na]^+$

Fig. S18. *High-resolution mass spectrometry (HRMS) from the comparison of the in vivo production of* ***8****.* This Fig. provides HRMS data from the peak indicated with the black dot in Fig. S15.

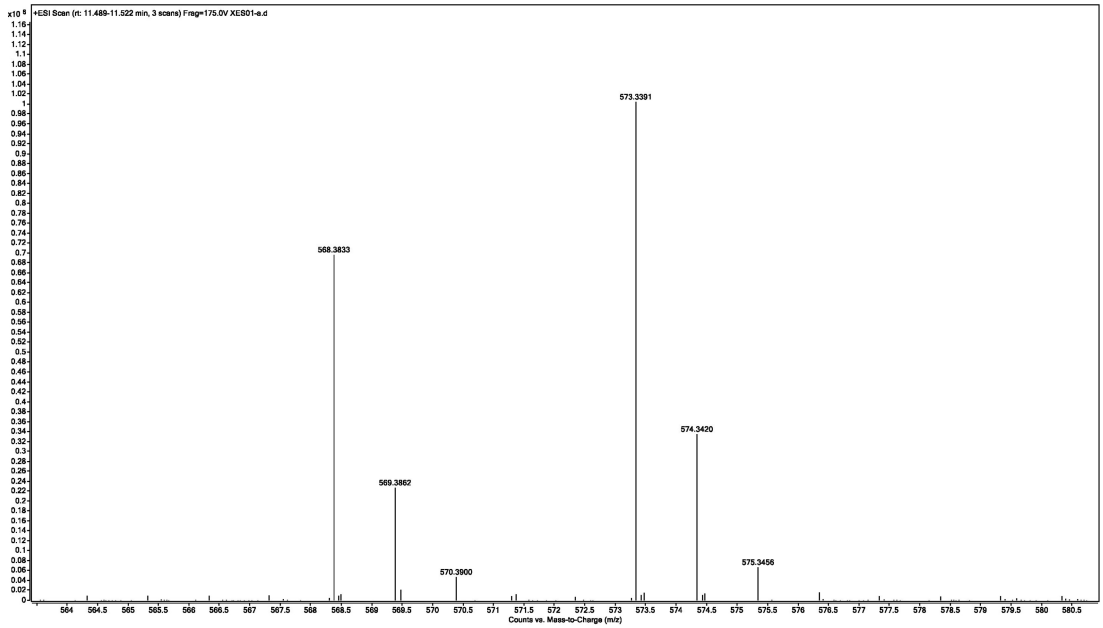

Search Results:

Mass Measured	Theo. Mass	Delta (ppm)	Composition
568.3833	568.3844	-1.9	$[C_{31}H_{50}O_8NH_4]^+$
573.3391	573.3398	-1.2	$[C_{31}H_{50}O_8Na]^+$

Fig. S19. *High-resolution mass spectrometry (HRMS) from the comparison of the in vitro production of* ***8****.* This Fig. provides HRMS data from the peak indicated with the black dot in Fig. S16.

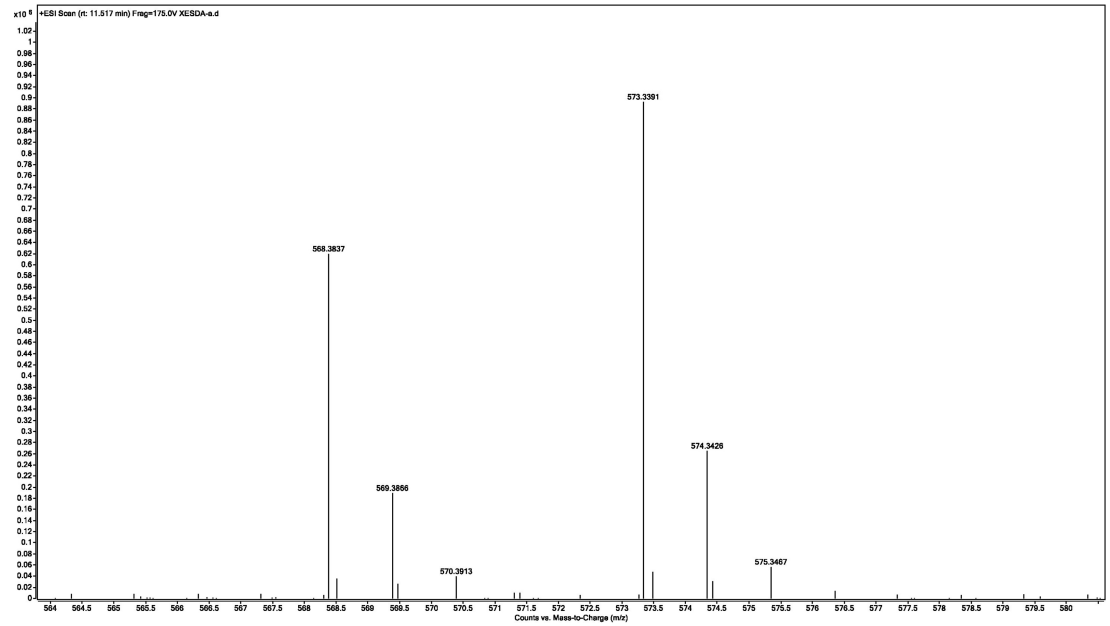

Search Results:

Mass Measured	Theo. Mass	Delta (ppm)	Composition
568.3837	568.3844	-1.2	$[C_{31}H_{50}O_8NH_4]^+$
573.3391	573.3398	-1.2	$[C_{31}H_{50}O_8Na]^+$

Fig. S20. *High-resolution mass spectrometry (HRMS) from the comparison of the in vivo and in vitro production of **8**.* This Fig. provides HRMS data from the peak indicated with the black dot in Fig. S17.

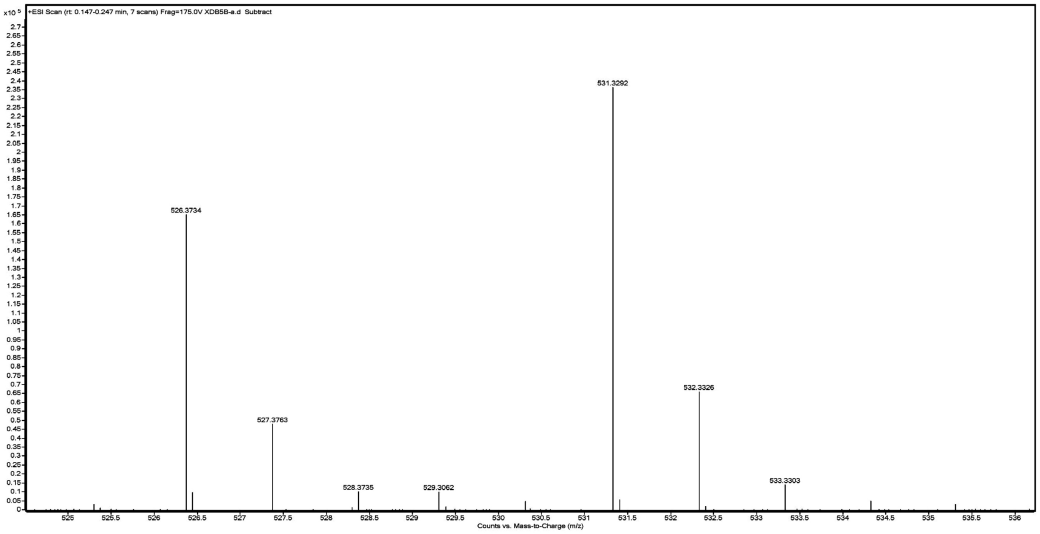

Sample XDB5B

Mass Measured	Theo. Mass	Delta (ppm)	Composition
526.3734	526.3738	-0.8	$[C_{29}H_{48}O_7NH_4]^+$
531.3292	531.3292	0.0	$[C_{29}H_{48}O_7Na]^+$

Fig. S21. *High-resolution mass spectrometry (HRMS) spectra of 7-desacetoxy-21-methoxypladienolide B (**9**).* Sodium (Na^+) and ammonium (NH_4^+) adducts precisely match the theoretical mass of **9** (508.3400), confirming the lack of an acetyl group.

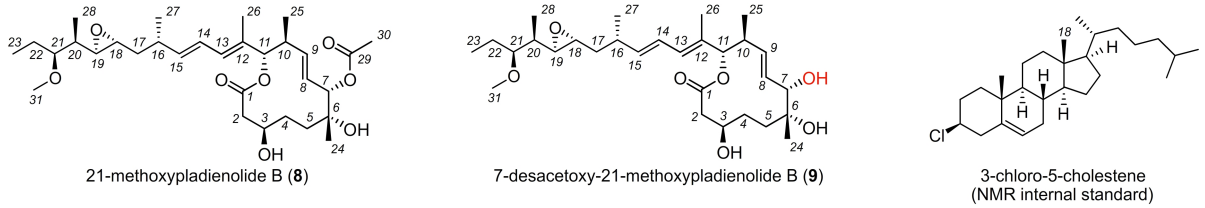

Fig. S22. *Compound numbering.* Structures and atom numbering for **8**, **9**, and the NMR internal standard 3-chloro-5-cholestene. The C18 methyl group of 3-chloro-5-cholestene provides an excellent signal for internal standardization.

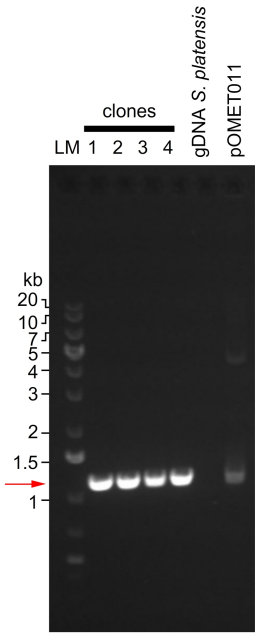

Fig. S23. *Clone validation.* PCR results of four individual *fddK* exconjugants of *S. platensis*. The expected band of the insert amplicon is 1,118 bp (red arrow). Exconjugant numbers are provided. pOMET011 (sequenced plasmid) was used as positive control. *S. platensis* (parent strain) gDNA was used as the negative control. Ladder, GeneRuler 1 kb Plus DNA Ladder (Thermo Fisher Scientific).

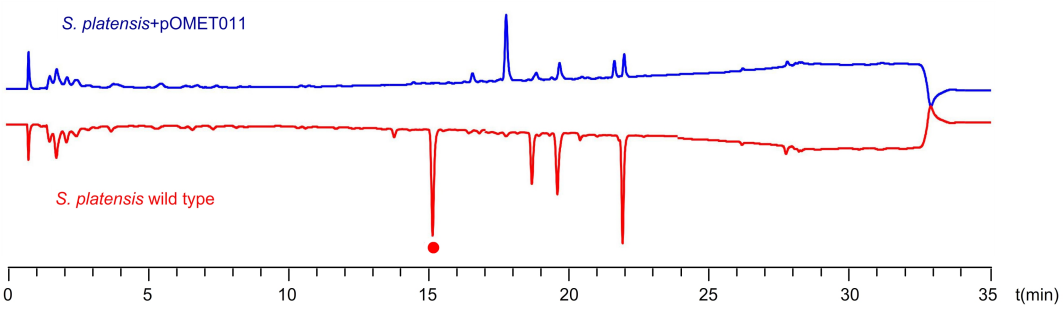

Fig. S24. *HPLC analyses of engineered strains.* HPLC chromatogram of *S. platensis* pOMET011 extract (blue) compared to the inverted chromatogram of wild-type (WT) extract (red). The pladienolide B (**2**) peak is highlighted with a red dot at 15.1 min. Detection at 240 nm. Both wild-type and engineered extracts contained pladienolide polyketides along with acyl-glycerides. We used a defatting procedure to remove most of the tri-acyl glycerides, but the di- and mono-acyl glycerides are readily seen by HPLC due to the presence of polyunsaturated fatty acids (PUFAs).

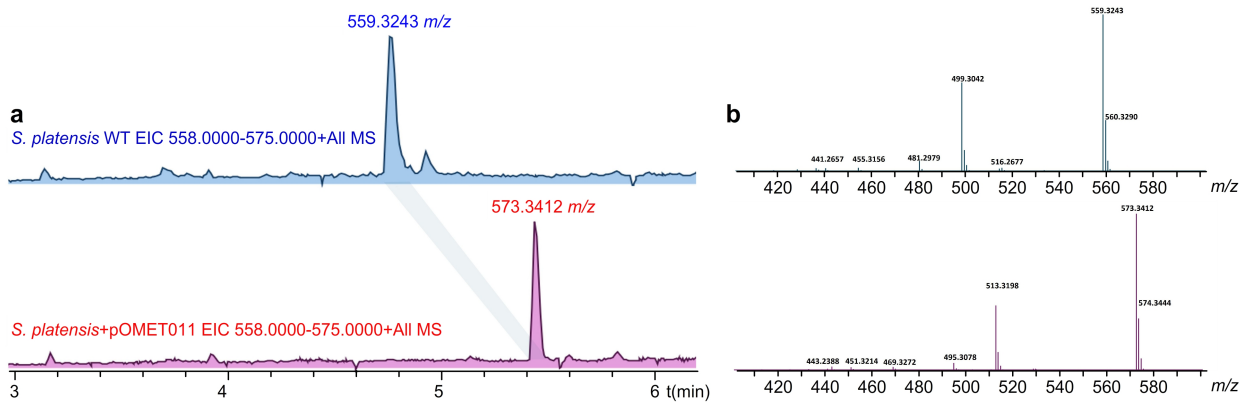

Fig. S25. *LC-MS analyses of engineered strains.* LC-MS chromatogram of *S. platensis* pOMET011 extract compared to the wild-type (WT) extract. **a)** Range of extracted ion chromatogram (558.000–575.000). The *fddK* mutant *S. platensis* pOMET011 (bottom) shows a *m/z* feature of 573.347 for the sodium adduct of the methylated pladienolide derivative as compared to pladienolide B (**2**) which was detected as a *m/z* feature of 559.335 for the sodium adduct in the wild type. **b)** Tandem mass spectrometry analysis of features corresponding to the sodium adducts of 21-methoxypladienolide B (**8**) (*m/z* 573.347, 5.5 min) in *S. platensis* pOMET011 (bottom) and pladienolide B (**2**) (*m/z* 559.335, 4.8 min, top) in the wild type (top), respectively.

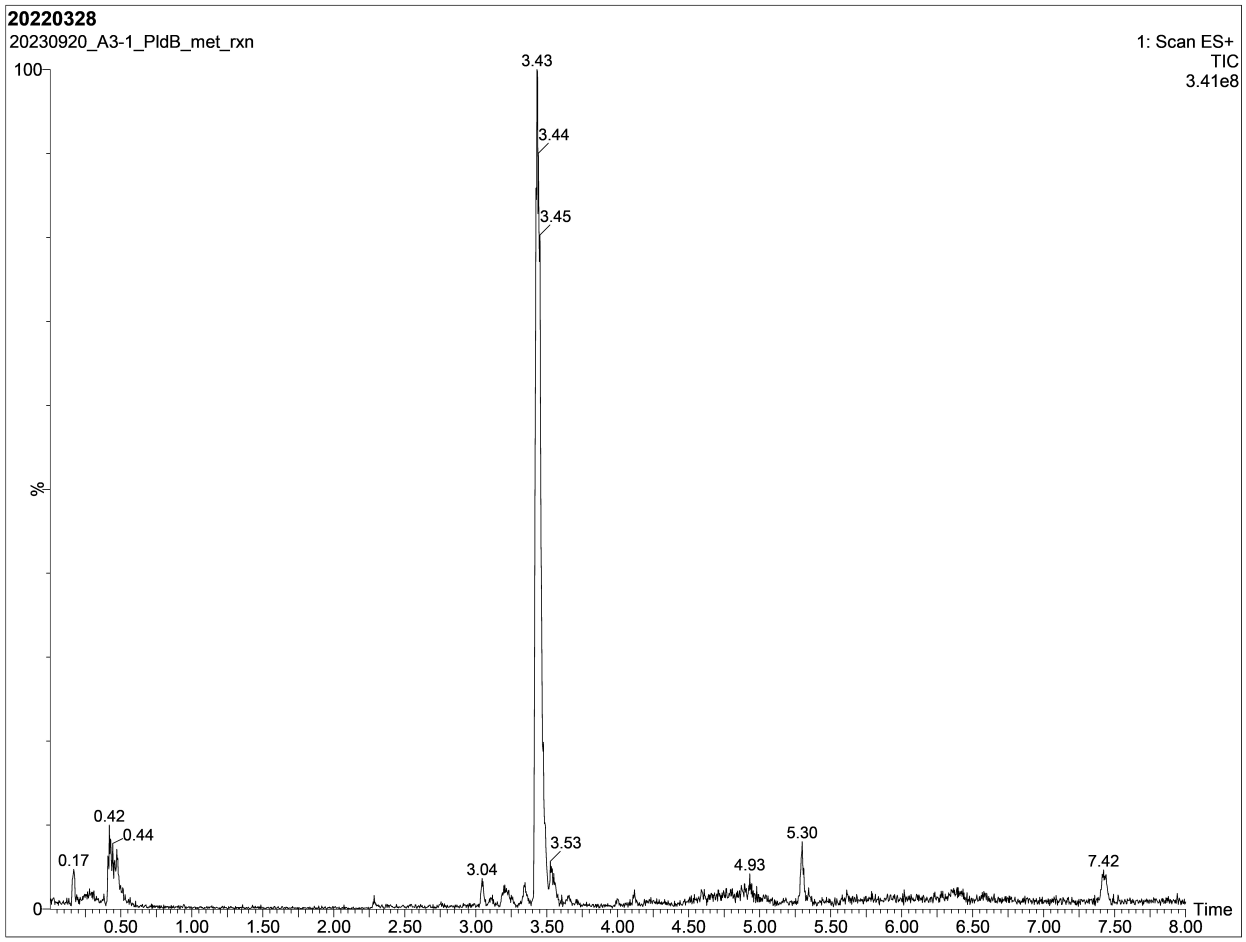

Fig. S26. *HPLC analysis of in vitro control reaction lacking enzyme, FddK.* Only the pladienolide B (**2**) peak is present (also demonstrated in Fig. S9 with corresponding MS data in Fig. S10).

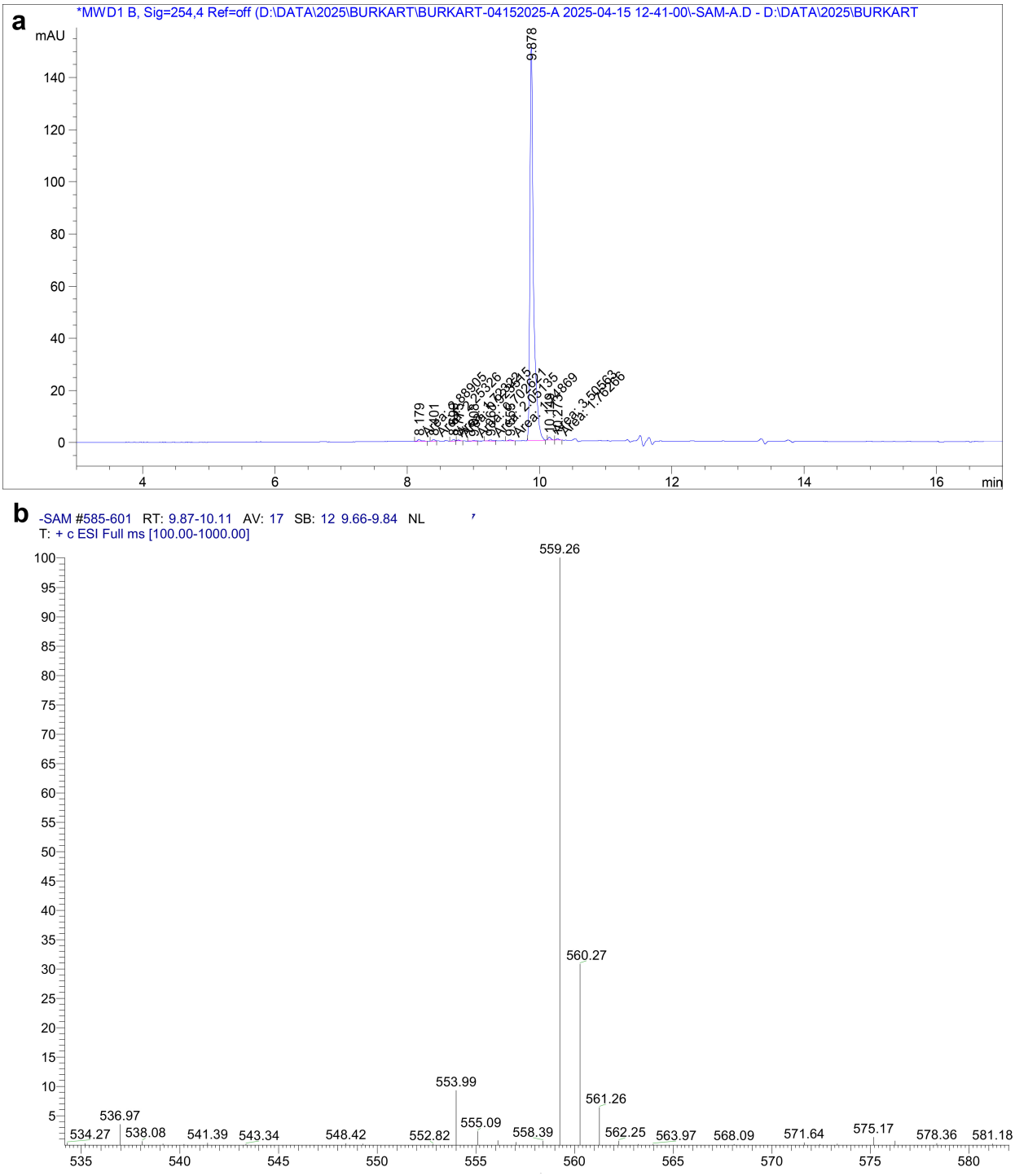

Fig. S27. *HPLC-MS analysis of in vitro control reaction lacking SAM.* **a)** HPLC trace demonstrating only one pain peak present. **b)** MS data from the main peak in part a confirms the ammonium, sodium, and potassium adducts of pladienolide B (**2**). 21-Methoxypladienolide B (**8**) was not detected.

Table S1. List of Oligonucleotide primers used in this study.

Primer Name	**Sequence 5'– 3'**
P1_herEF_F	*GGAATTC*CATATGCACACCGACTCACCTACG
P2_herEF_R	*GC*TCTAGAGTCTCGGTCATGGTGTCG
P1_NdeI_herF_F	*ATAGCG*CATATGCACGGAAAACGGAACAGGACA
P2_XbaI_herF_R	*TTGAGG*TCTAGAAGGTCTCGGTCATGGTGTCG
TP_herEF_1_R	TGACATTGGGGAATTTATGC
TP_herEF_2_F	GTTGTGTGGAATTGTGAGC
TP_herEF_3_F	CAGTACGTCATCACCTGC
TP_herEF_4_F	AACTCTCCCTCTGGCCCG
TP_herF_MID_R	TTCGTGATCTGTTCCCGGC
P1_herEF_noext_F	CACACCGACTCACCTACG
P2_herEF_noext_R	GTCTCGGTCATGGTGTCG
P1_herF_noext_F	ACGGAACAGGACACCACG
P2_herF_noext_R	GTCTCGGTCATGGTGTCG
P1 P_ermE*_F	*GA*AGATCTGTGCACGCGGTCGATCTTG
P2 P_ermE*_R	**CGTAAAGGCCTCCGAACTGC**CACCGCTGGATCCTACCAAC
P3 P_O-metase_F	GCAGTTCGGAGGCCTTTACG
P4 P_O-metase_R	*GC*TCTAGAGGTTTCACAGACACCGTCGC

Restriction sites are underlined. Extra sequences inserted to allow efficient restriction of PCR fragments are in *italics*. The overhang sequence inserted for SOE-PCR is in bold.

Table S2. Summary of Atomic Sort results to evaluate *herF* and *herEF* expression in *S. platensis* Mer-11107. Precursor refers to the alkene precursor (lacks epoxidation) to pladienolide B (**2**). Genes *herE* and *herF* encode epoxidase and *O*-methyltransferase in the herboxidiene pathway. d_{AS} is the Atomic Sort distance, where a smaller number indicates a better match. The structures shown in the observed atoms column correspond to the precursor (upper) and pladienolide B (**2**) (lower). Atoms identified by Atomic Sort are shown in full color. Atoms not identified are transparent. The Atom column indicates which atom was used to estimate concentrations from integrals. The benzene concentration of 60.8 mM for the residual protonated solvent peak was calculated from the solvent suppliers deuteration specification and the density of benzene.

culture	molecule	median d_{AS}	atoms observed	atom	integral	concentration (mM)	average	std dev
WT isolate	Benzene	0.030	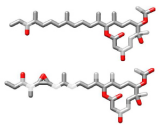	C1	142.521	60.8	60.8	
0N10N3	Precursor	0.123		C19	6.65371	17.0	16.7	0.5
				C18	6.35779	16.3		
	Pladienolide B	0.188		C19	5.66262	14.5	17.5	4.2
				C18	7.99809	20.5		
herF 2	Benzene	0.009	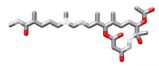	C1	202.214	60.8	60.8	
	Precursor	0.093		C19	1.0755	1.9	2.0	0.1
				C18	1.12466	2.0		
	Pladienolide B	0.121	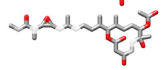	C19	1.61782	2.9	3.2	0.4
				C18	1.94812	3.5		
herF 5	Benzene	0.008	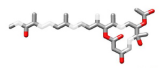	C1	183.25	60.8	60.8	
	Precursor	0.146		C19	-	-	-	-
				C18	-	-		
	Pladienolide B	0.125	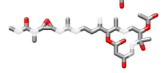	C19	1.43278	2.9	3.1	0.4
				C18	1.71907	3.4		
herF 6	Benzene	0.004	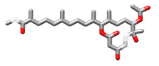	C1	182.909	60.8	60.8	
	Precursor	0.078		C19	1.76756	3.5	3.3	0.3
				C18	1.58319	3.2		
	Pladienolide B	0.109	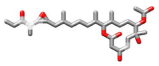	C19	3.59314	7.2	7.5	0.4
				C18	3.88319	7.7		
herF 16	Benzene	0.023	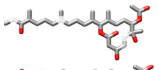	C1	170.176	60.8	60.8	
	Precursor	0.094		C19	2.07148	4.4	4.6	0.2
				C18	2.18092	4.7		
	Pladienolide B	0.159	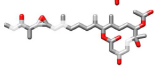	C19	2.24283	4.8	5.2	0.5
				C18	2.60039	5.6		
herEF 2	Benzene	0.001	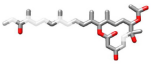	C1	151.253	60.8	60.8	
	Precursor	0.143		C19	-	-	-	-
				C18	-	-		
	Pladienolide B	0.115	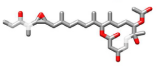	C19	5.88851	14.2	14.0	0.2
				C18	5.74648	13.9		
herEF 5	Benzene	0.007	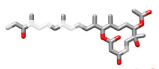	C1	151.357	60.8	60.8	
	Precursor	0.134		C19	-	-	-	-
				C18	-	-		
	Pladienolide B	0.095	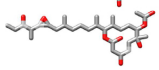	C19	7.89976	19.0	19.5	0.7
				C18	8.29169	20.0		
herEF 6	Benzene	0.003	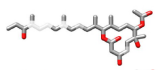	C1	151.357	60.8	60.8	
	Precursor	0.134		C19	-	-	-	-
				C18	-	-		
	Pladienolide B	0.078	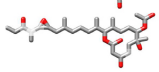	C19	7.37179	17.8	19.3	2.2
				C18	8.65031	20.8		
herEF 8	Benzene	0.006	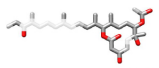	C1	147.959	60.8	60.8	
	Precursor	0.204		C19	-	-	-	-
				C18	-	-		
	Pladienolide B	0.117	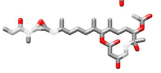	C19	2.93751	7.2	8.0	1.0
				C18	3.5158	8.7		
SPCGB	Benzene	0.011		C1	147.959	60.8	60.8	
	Precursor	-						
	Pladienolide B	-						

Table S3. *In vitro temperature study data.* The left column includes the reaction temperatures throughout the temperature study, while the right column shows the corresponding integration value of the C21-methoxy peak of **8** relative to the C18 peak of 3-chloro-5-cholestene from the ^{1}H NMR spectra of the crude reactions.

Temperature (°C)	Integration of C21-methoxy peak of **8**
50	0.43
45	0.66
42	0.69
40	0.76
37	0.51
35	0.35
30	0.22
25	0.17
20	0.07

Table S4. *In vitro pH study data.* The left column includes the reaction pH throughout the pH study, while the right column shows the corresponding relative integration value of the C21-methoxy peak of **8** from the ^{1}H NMR spectra of the crude reactions.

pH	Integration of C21-methoxy peak of **8**
8.0	0.87
7.7	0.70
7.5	0.89
7.3	0.56
7.0	0.47

Table S5. NMR data for 21-methoxypladienolide (**8**) in C_6D_6 [a]

Position[a]	δ_H, mult (*J* in Hz)	δ_C	^{1}H, ^{1}H-COSY
1		172.1	
2’	2.29, dd (14.8, 3.7)	38.3	2’’, 3w
2’’	2.19, dd (14.8, 2.9)		2’, 3w
3	3.50, m	69.1	2’w, 2’’w, 3OHw
3OH	3.66, m		3
4’	1.56, m	30.4	4’’,5’,5’’
4’’	1.21, m		4’, 5’,5’’
5’	1.56, m	35.9	4’, 4’’,5’’
5’’	1.21, m		4’, 4’’,5’
6		73.3	
6OH	1.85, s		
7	5.25, d (9.8)	79.0	8
8	5.82, dd (15.3, 9.8)	126.2	7, 9
9	5.62, dd (15.2, 10.0)	140.4	8, 10
10	2.39, m	40.8	9,11, 25
11	5.27, d (10.7)	82.5	10
12		131.6	
13	6.13, dd (10.8, 1.3)	131.5	14, 26
14	6.23, dd (14.9, 10.8, 1.0)	124.4	13, 15
15	5.45, dd (14.9, 8.4)	141.7	14, 16w
16	2.33, m	35.5	17’,17’’, 27
17’	1.48, ddd (13.7, 6.4, 5.3)	39.8	16, 17’’, 18
17’’	1.37, m		16, 17’, 18
18	2.55, ddd (6.4, 5.4, 2.2)	56.7	17’, 17’’,19
19	2.67, dd (8.1, 2.1)	61.0	18, 20
20	1.29, m	39.4	19, 21, 28
21	3.15, td (6.4, 4.0)	83.4	20, 22’w
22’	1.65, m	23.7	22’’, 23
22’’	1.40, m		22’, 23
23	0.85, t (7.3)	9.8	22’, 22’’
24	1.00, s	24.5	
25	0.71, d (6.7)	16.1	10
26	1.57, d (1.3)	11.5	
27	1.14, d (6.8)	17.0	16
28	0.83, d (7.1)	10.6	20
29		168.9[a]	
30	1.60, s	20.5	
31	3.27, s	57.6	

[a] Position numbering is provided in Fig. S22. Letter w denotes that the cross peak is weak.

Table S6. Inhibition of cell proliferation (EC_{50} values).

EC_{50} values (% Cell Viability)		
	OVCAR3 (nM)	**OV81.2 (nM)**
pladienolide B (**2**)	1.22 ± 0.21	0.71 ± 0.05
21-methoxypladienolide B (**8**)	1.88 ± 0.12	3.28 ± 0.35
17*S*-FD-895 (**4**)	1.07 ± 0.10	1.10 ± 0.12
Taxol (positive control)	3.42 ± 0.09	6.14 ± 0.14

^{1}H-NMR characterization of the enzymatic yield of 21-methoxypladienolide B (**8**) in C_6D_6

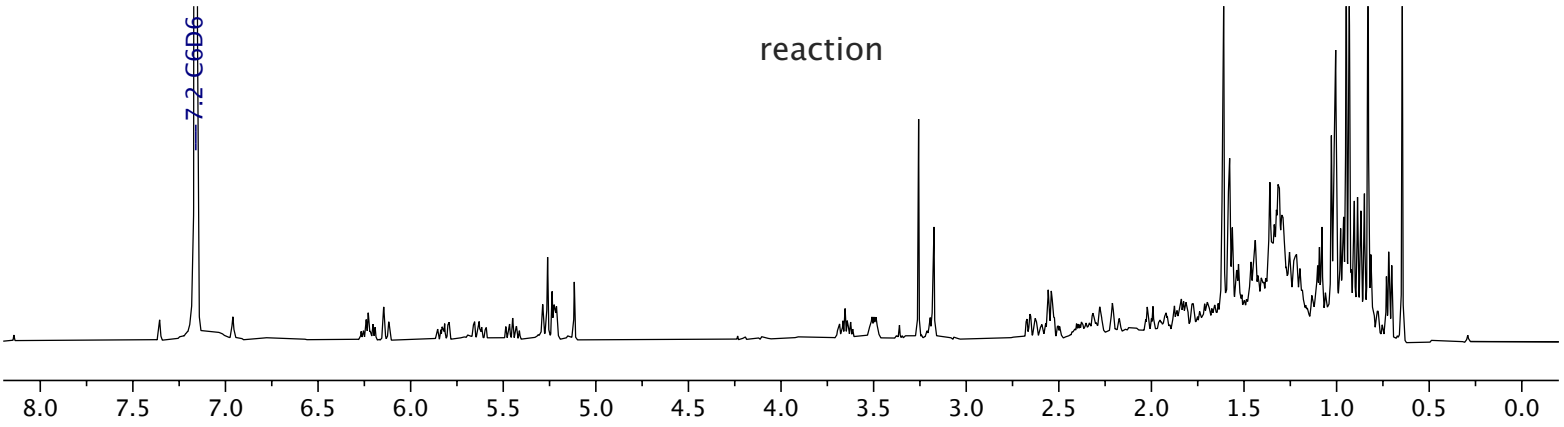

3-chlorocholesterol (internal standard)

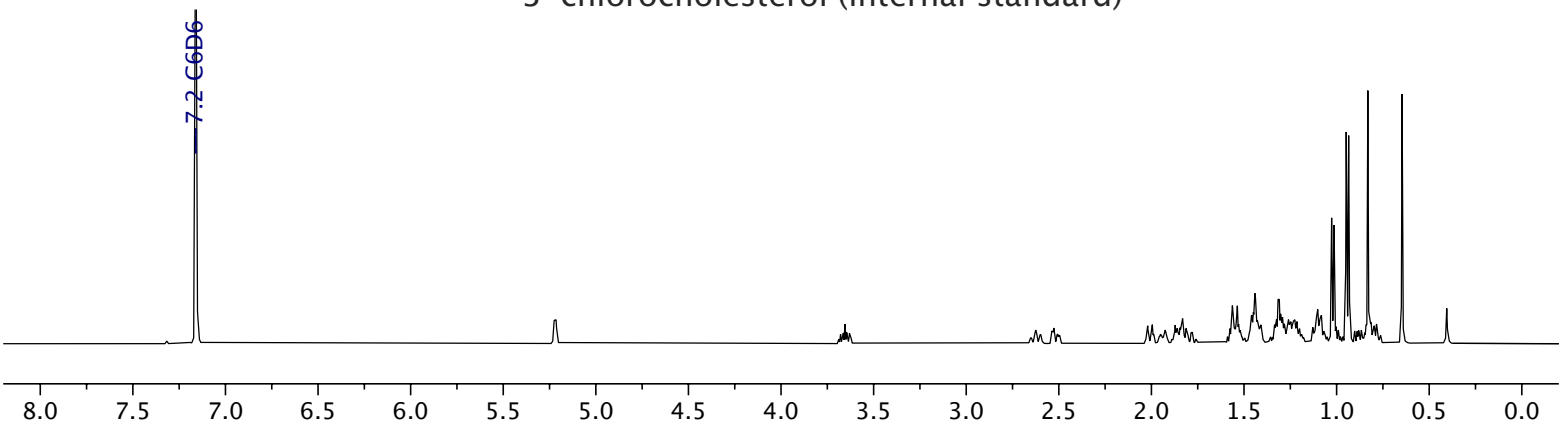

pladienolide B (**2**, starting material)

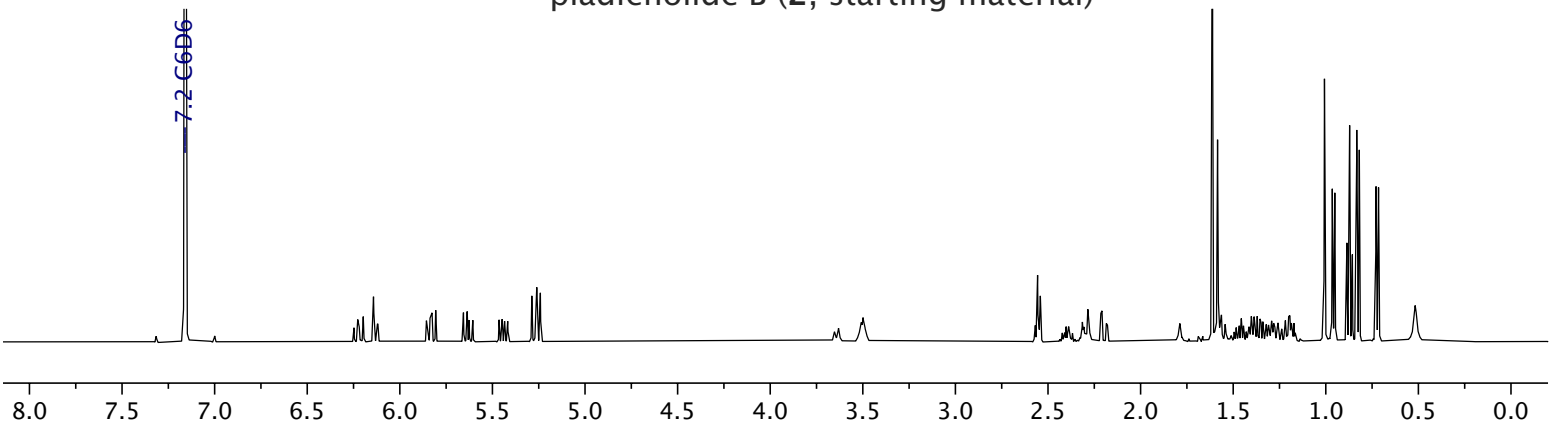

21-methoxypladienolide B (**8**, product)

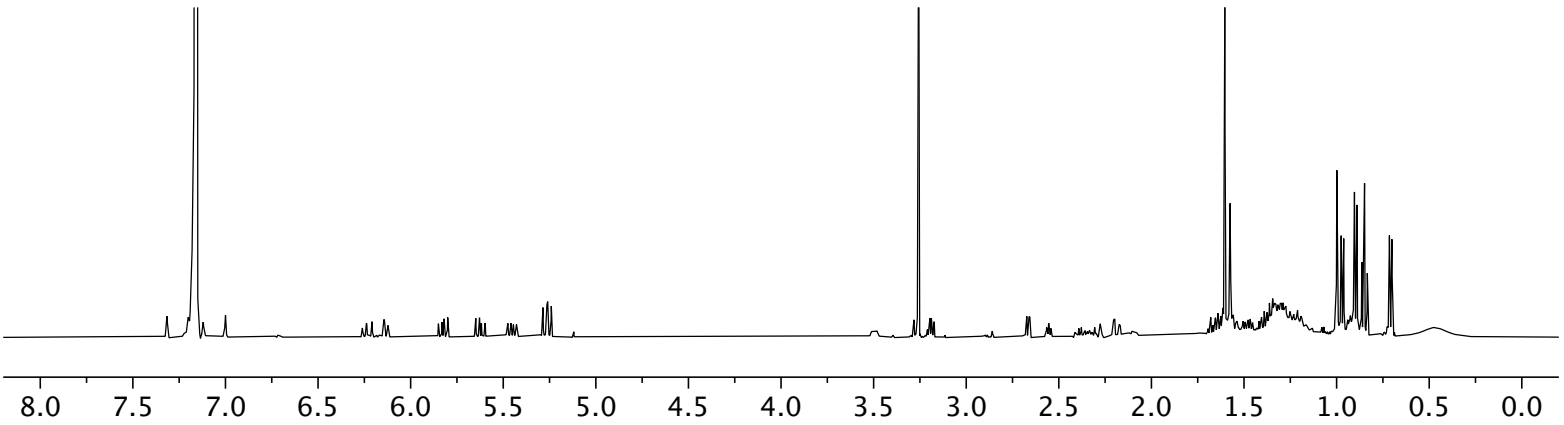

^{1}H-NMR characterization of the enzymatic yield of 21-methoxypladienolide B (**8**) in C_6D_6

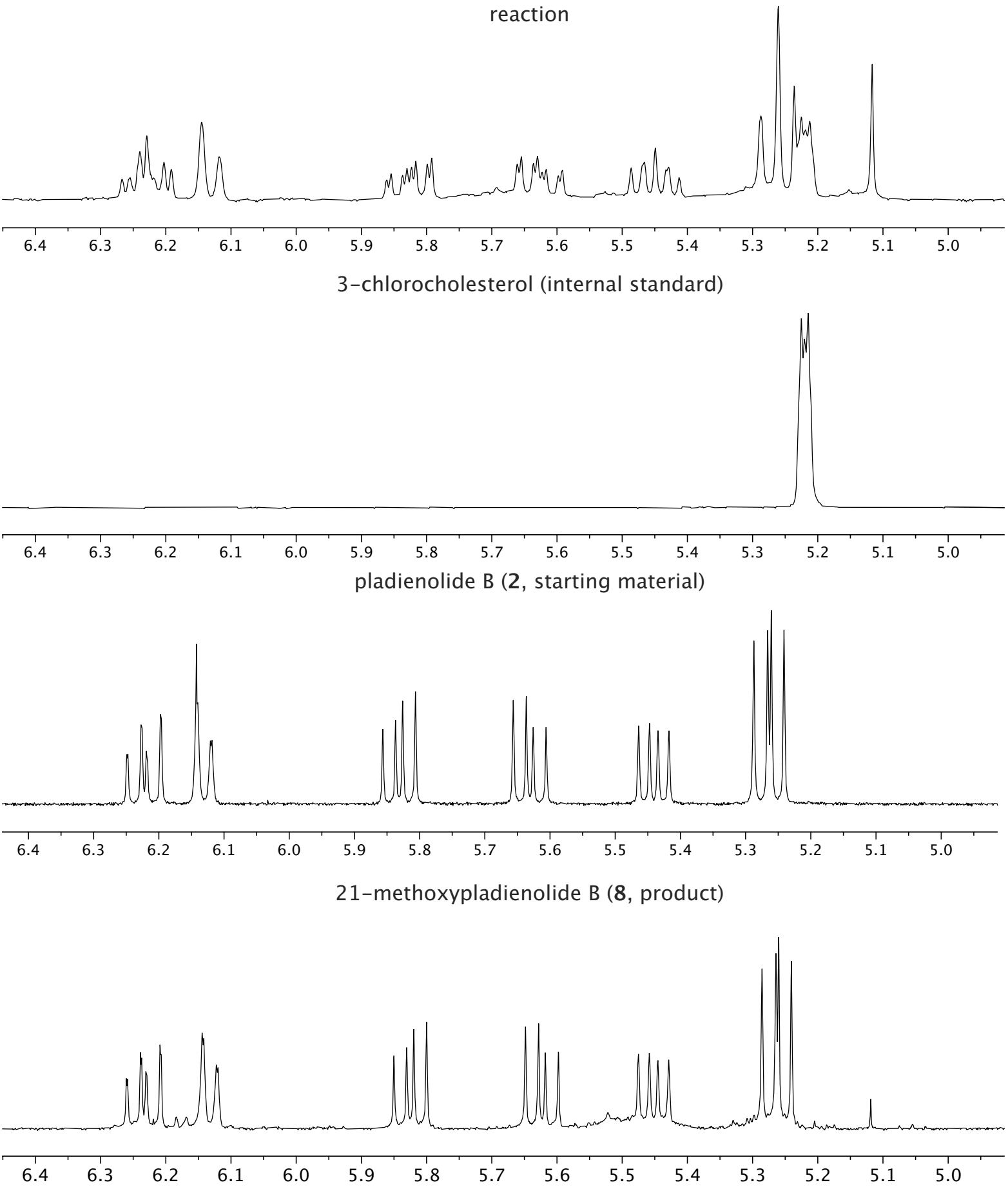

^{1}H-NMR characterization of the enzymatic yield of 21-methoxypladienolide B (**8**) in C_6D_6

reaction

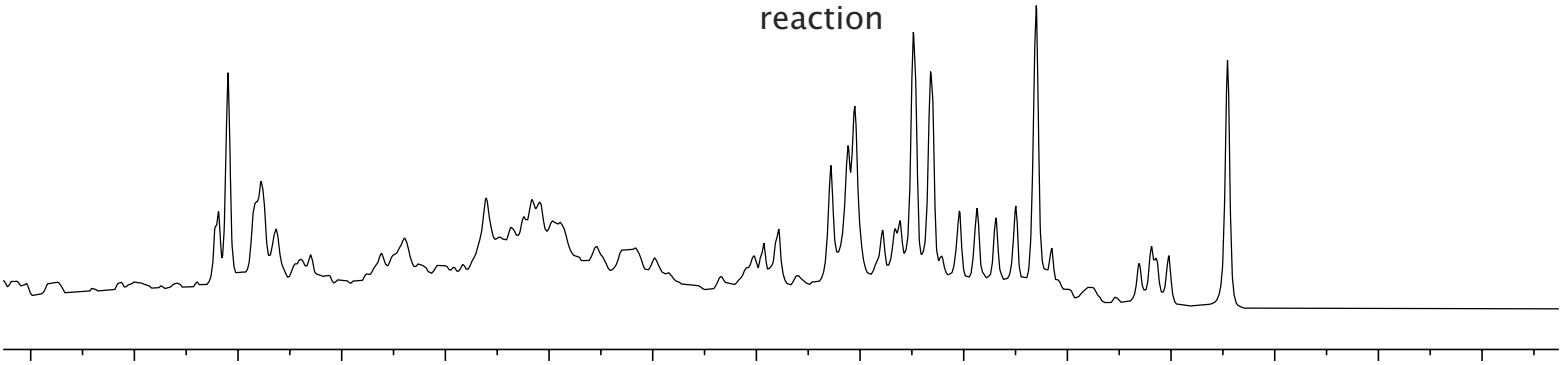

3-chlorocholesterol (internal standard)

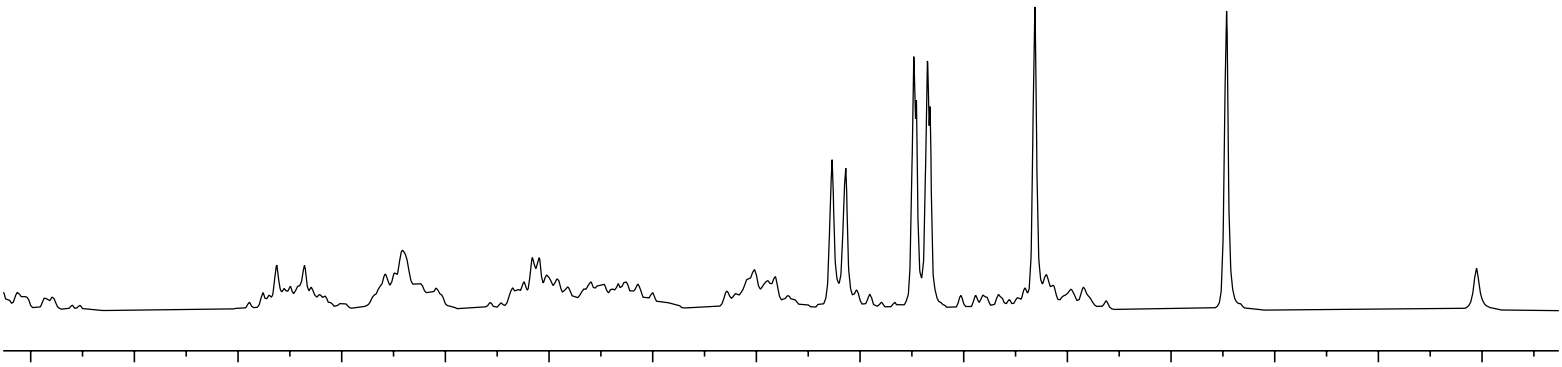

pladienolide B (**2**, starting material)

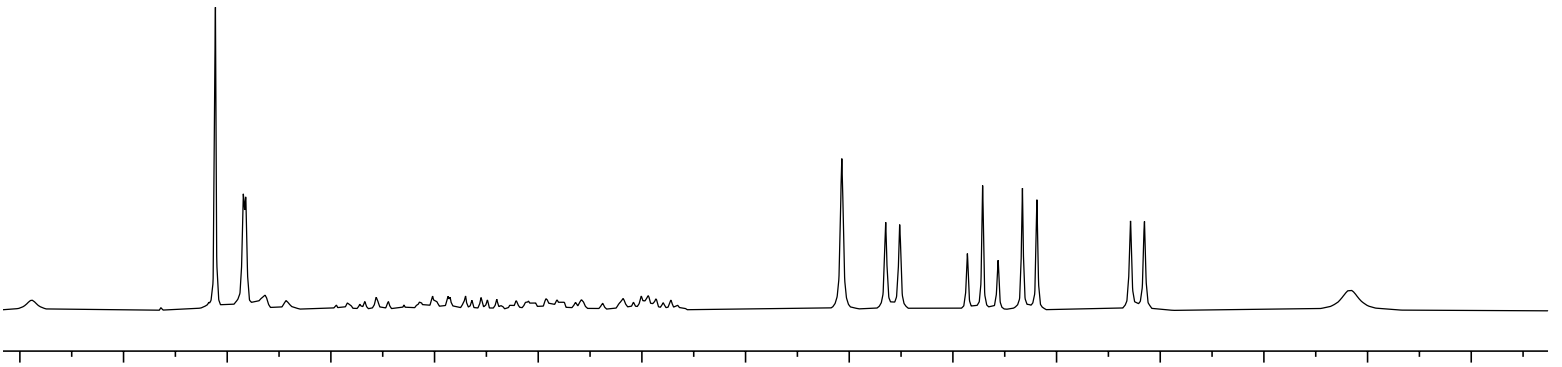

21-methoxypladienolide B (**8**, product)

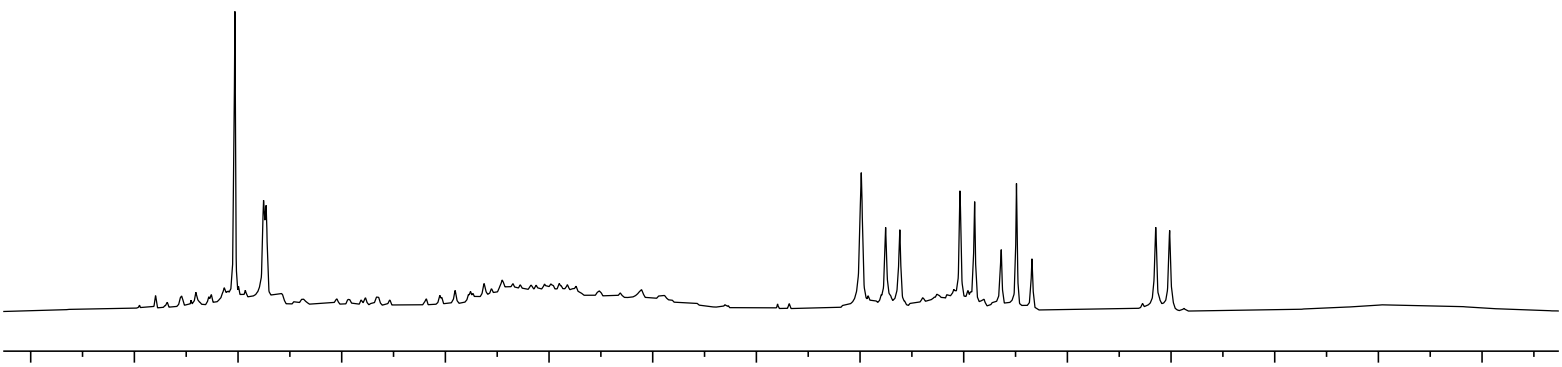

^{1}H-NMR (400 MHz) spectrum of 21-methoxypladienolide B (**8**) in C_6D_6

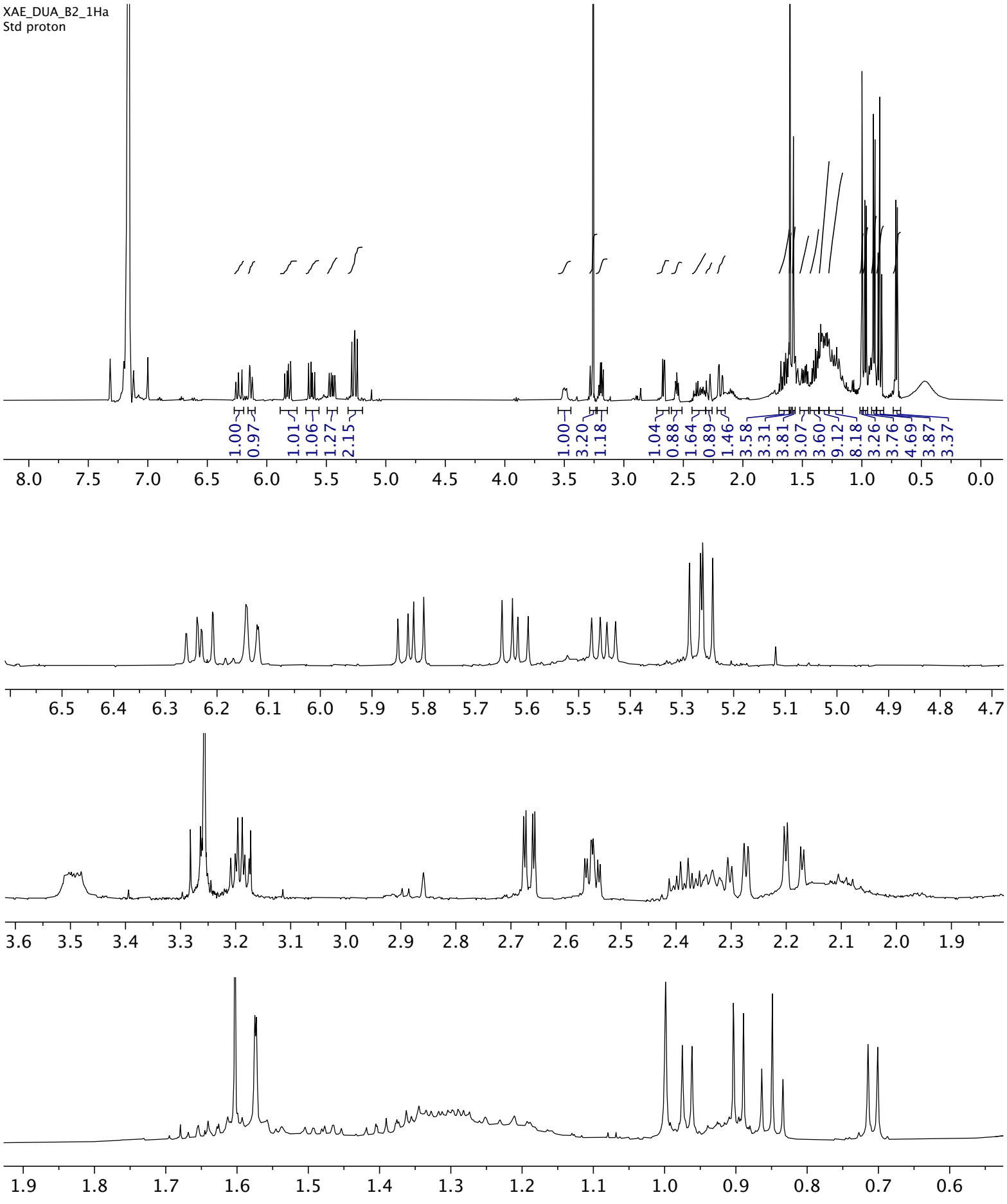

$^{1}H,^{1}H$-gCOSY spectrum (400 MHz) of 21-methoxypladienolide B (**8**) in C_6D_6

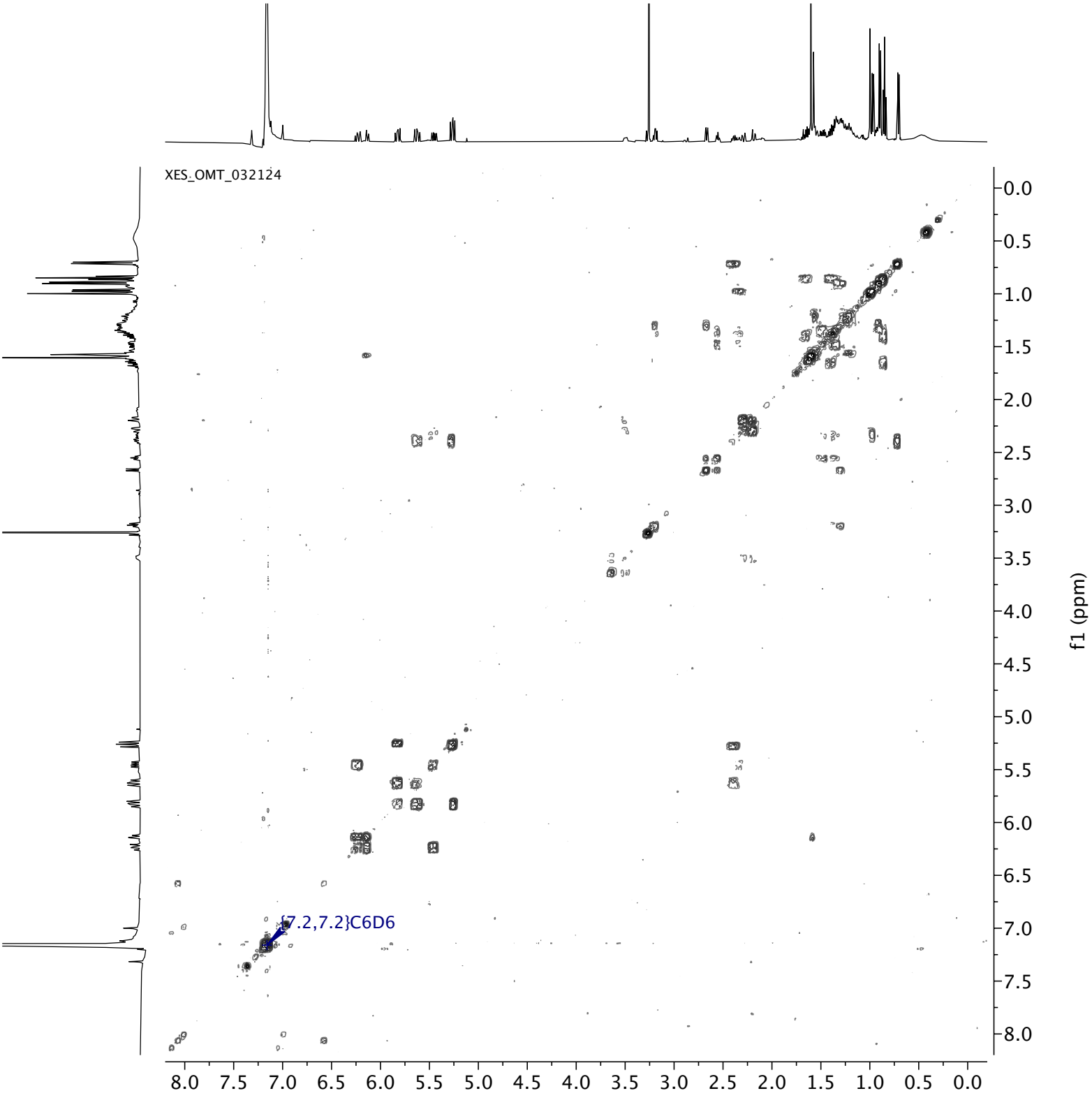

$^{1}H,^{13}C$-HSQC spectrum (400 MHz) of 21-methoxypladienolide B (**8**) in C_6D_6

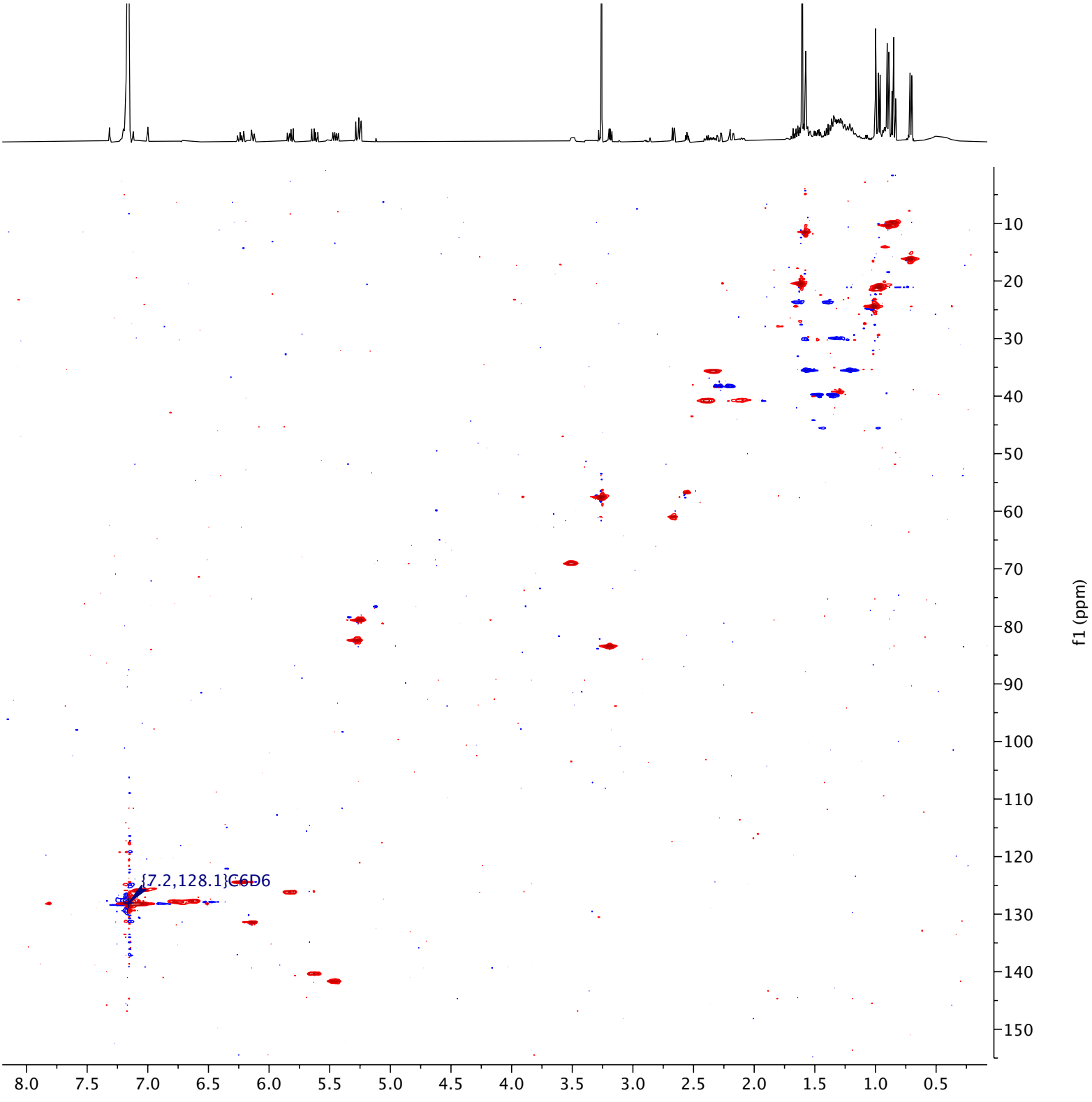

$^{1}H,^{13}C$-HMBC spectrum (400 MHz) of 21-methoxypladienolide B (**8**) in C_6D_6

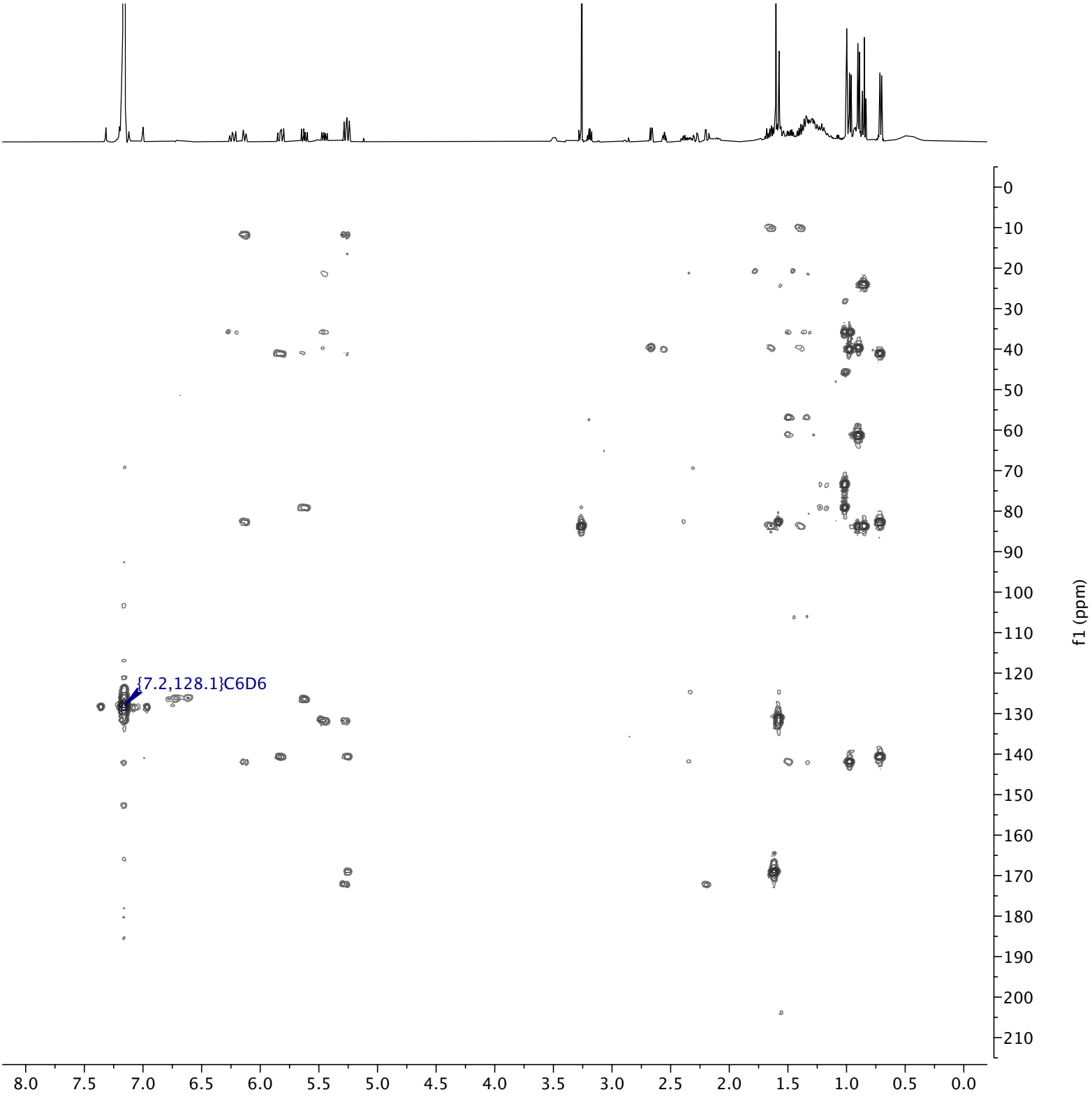

^{1}H-NMR (400 MHz) spectrum of 7-desacetoxy-21-methoxypladienolide B (**9**) in C_6D_6

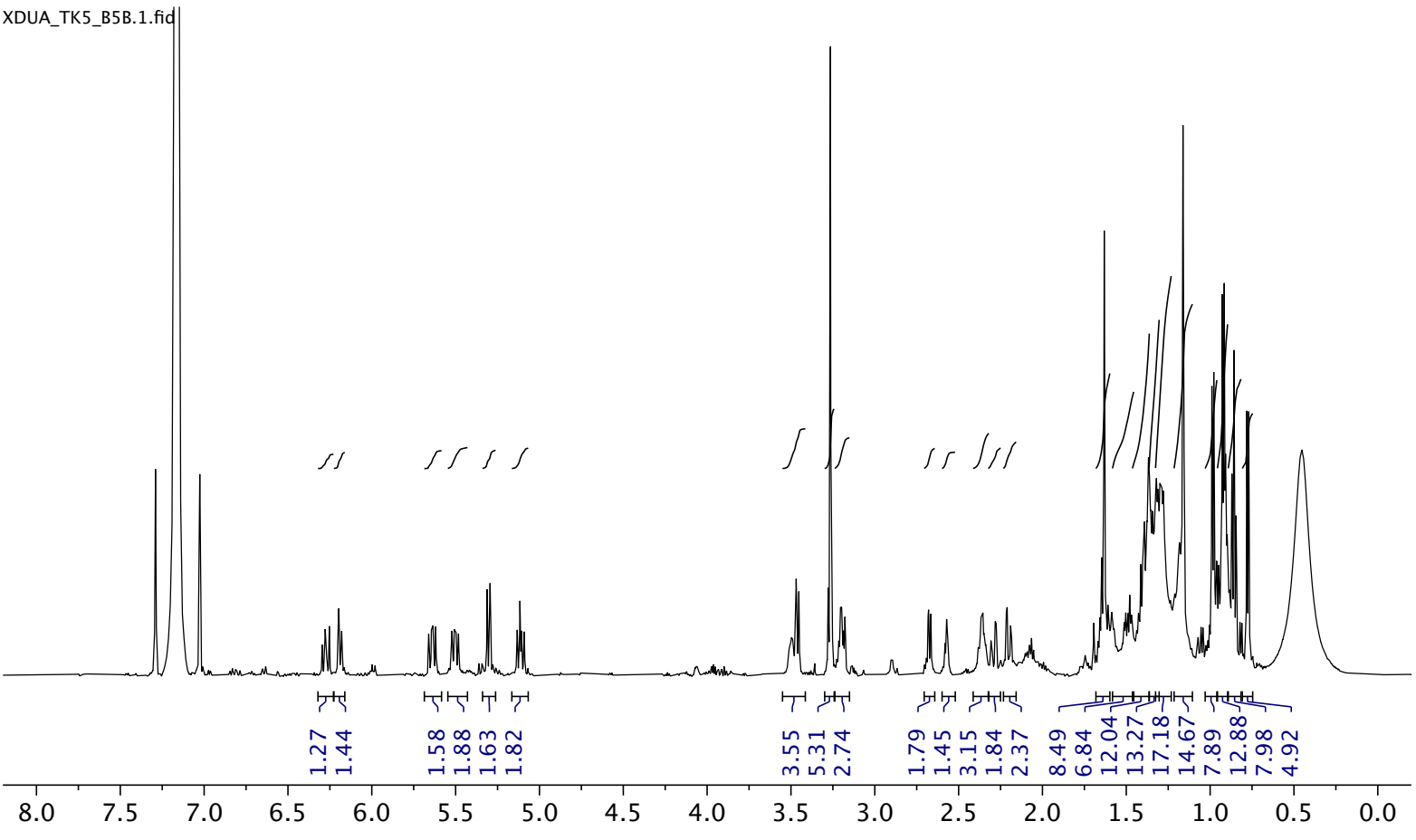

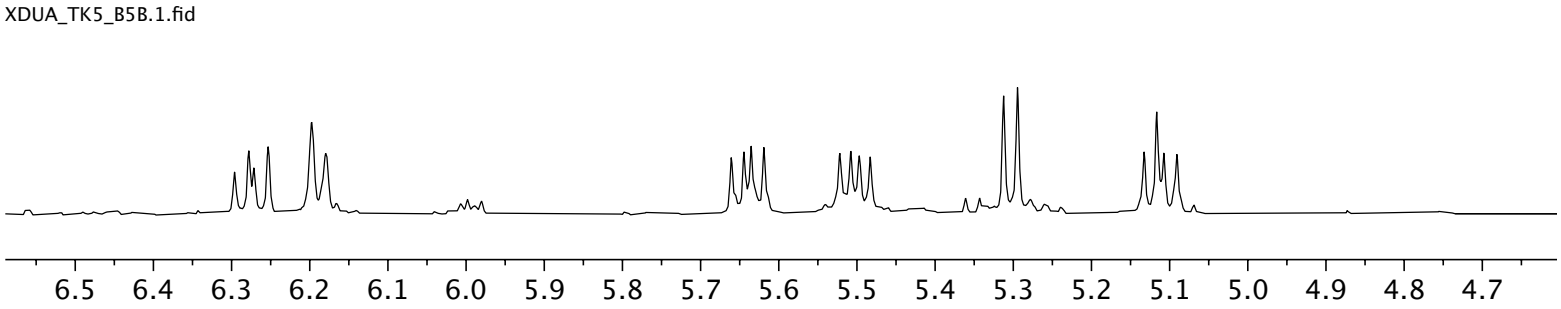

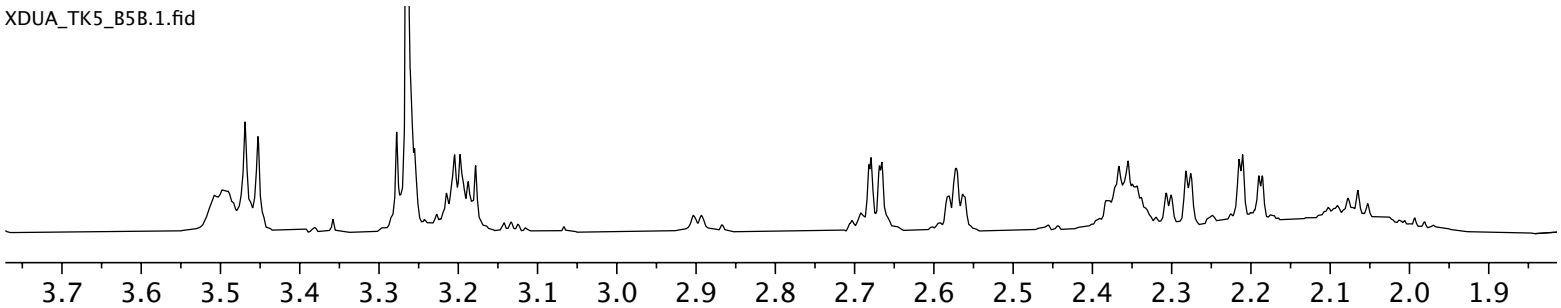

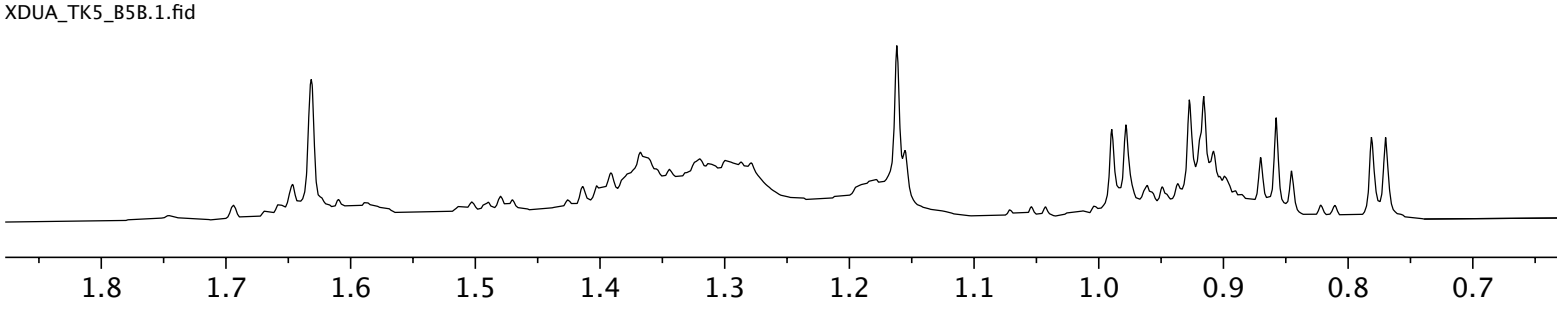

$^{1}H,^{1}H$-gCOSY spectrum (400 MHz) of 7-desacetoxy-21-methoxypladienolide B (**9**) in C_6D_6

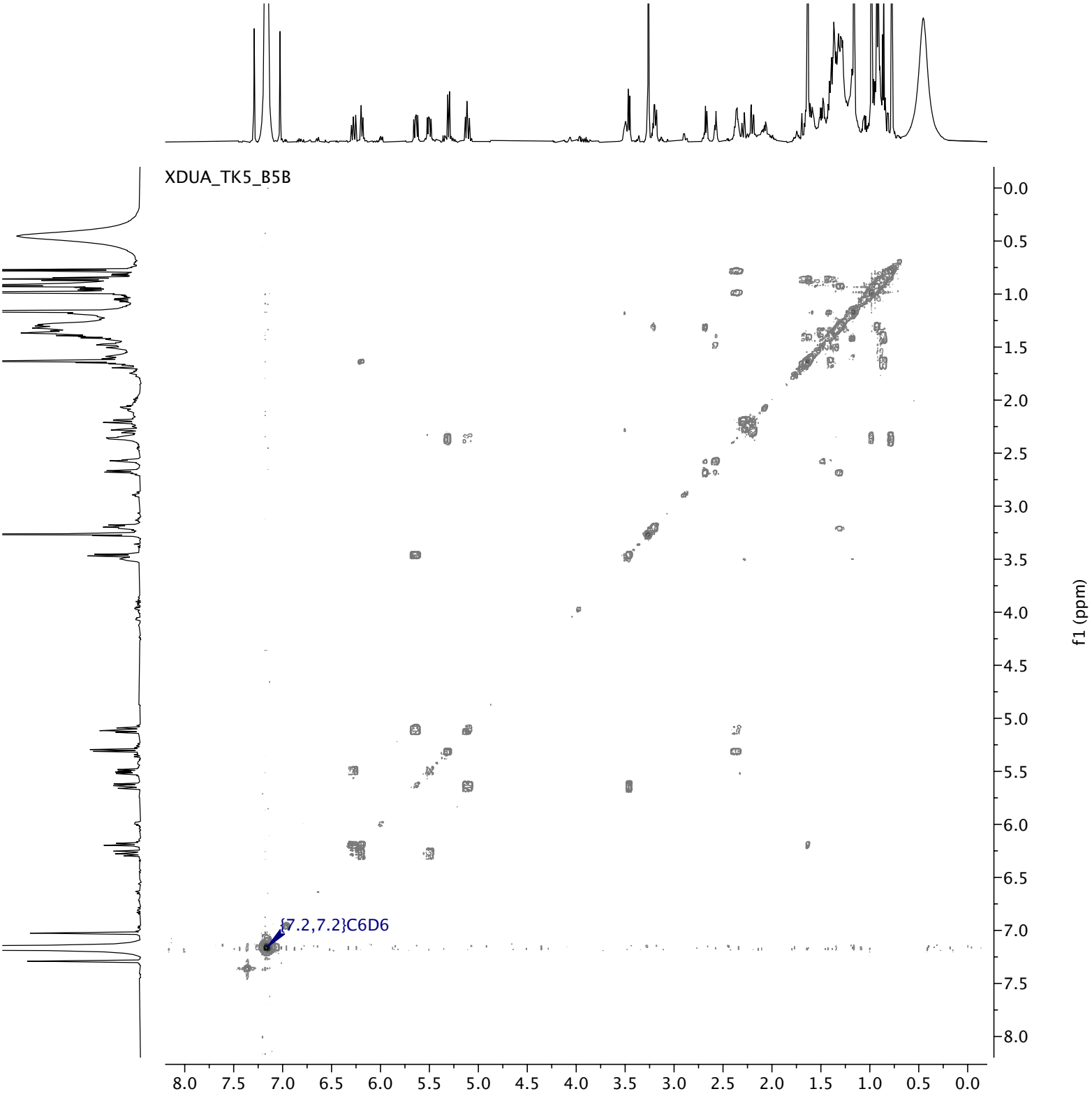

$^{1}H,^{13}C$-HSQC spectrum (400 MHz) of 7-desacetoxy-21-methoxypladienolide B (**9**) in C_6D_6

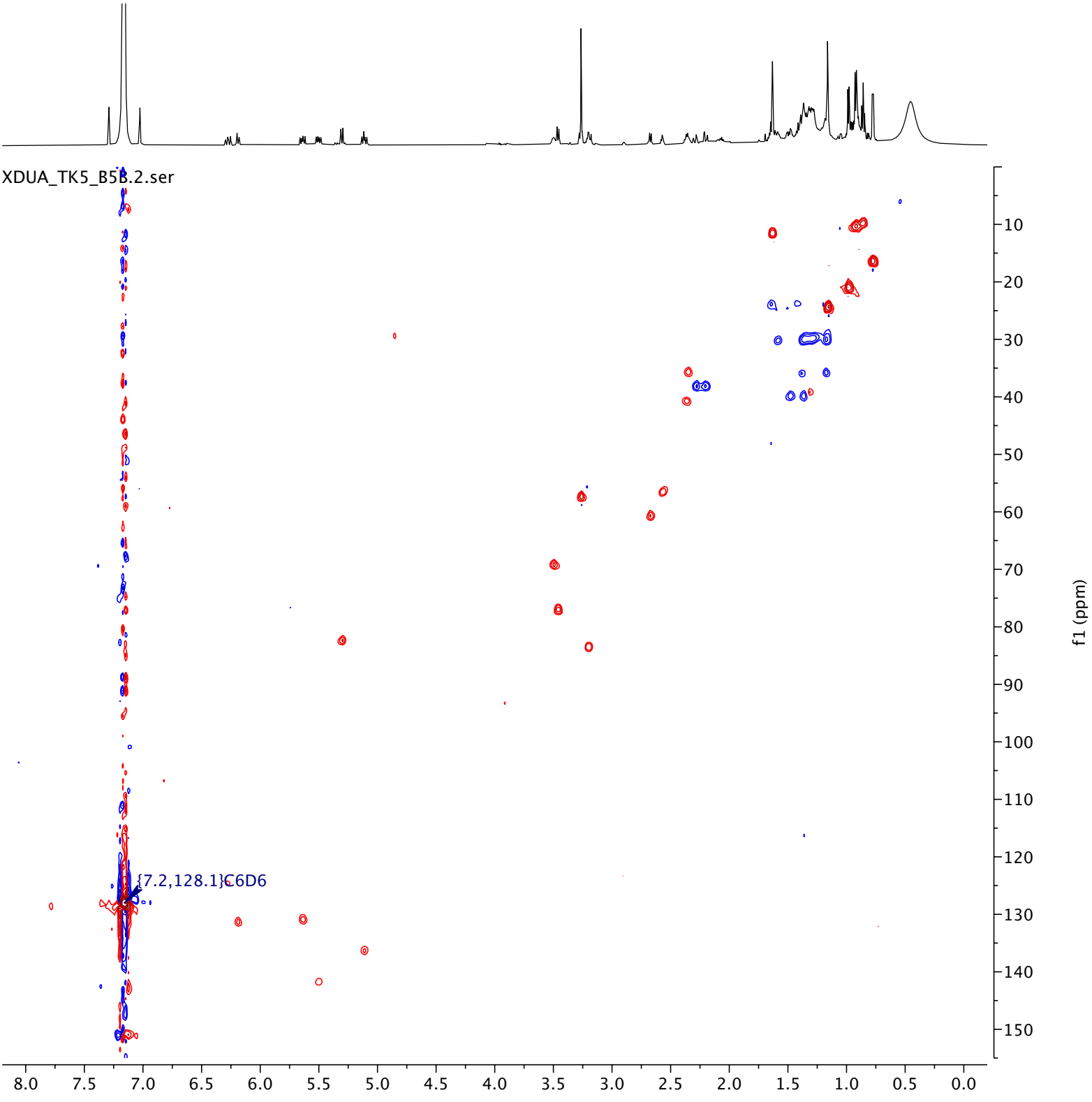

$^{1}H,^{13}C$-HSQC spectrum (600 MHz) of 7-desacetoxy-21-methoxypladienolide B (**9**) in C_6D_6